International Journal of Heat and Mass Transfer 190 (2022) 122579

Contents lists available at ScienceDirect

International Journal of Heat and Mass Transfer

journal homepage: www.elsevier.com/locate/hmt

Review of Cryogenic Pool Boiling Critical Heat Flux Databases, Assessment of Models and Correlations, and Development of New Universal Correlations

Raj Patel[a], Michael Meyer[b], Jason Hartwig[c], Issam Mudawar[a,b,*]

[a] Purdue University Boiling and Two-Phase Flow Laboratory (PU-BTPFL), School of Mechanical Engineering, Purdue University, 585 Purdue Mall, West Lafayette, IN 47907, U.S.A.
[b] MTS Inc., 3495 Kent Ave, Suite F, West Lafayette, IN 47906, U.S.A.
[c] NASA Glenn Research Center, Fluids and Cryogenics Branch, Cleveland, OH 44135, U.S.A.

ARTICLE INFO

Article history:
Received 11 December 2021
Revised 11 January 2022
Accepted 12 January 2022
Available online 28 March 2022

Keywords:
Pool boiling
Critical heat flux
Cryogens
Models
Correlations

ABSTRACT

Despite worldwide interest in a number of applications involving cryogenic fluids that are crucial to future space exploration, there is presently a lack of a large, reliable cryogenic pool boiling critical heat flux (CHF) database that can be used for assessment of accuracy of available predictive tools - model and correlations – or development of new tools. This shortcoming is a primary motivation for the present study, prompting compilation of a new consolidated cryogenic pool boiling CHF database from world literature. The database is used to assess accuracy of previous models and correlations, which are segregated according to ability to predict key operating parameters, such as pressure, surface orientation, and subcooling. A new correlation is constructed which shows very good predictive accuracy, evidenced by a mean absolute error of 16.95%, based on Earth gravity data which comprise a large fraction of the consolidated database. Using a limited subset of datapoints for three cryogens and a reduced gravity range of 0–0.7466, the new correlation is further modified with a reduced gravity multiplier to tackle reduced gravity conditions. The modified correlation has a mean absolute error of 17.47%, slightly higher than for Earth gravity alone. Overall, the new correlations are proven far more accurate than all prior models and correlations and therefore constitute new powerful tools in the quest for constructing universal flow boiling models for design of cryogenic space systems. It is shown CHF is very sensitive to pressure, increasing with increasing pressure up to a maximum before decreasing appreciably toward critical pressure. CHF is also shown to be strongly influenced by surface orientation, being highest for horizontal surfaces and decreasing monotonically with increasing orientation angle, and increasing fairly linearly with increased subcooling.

1. Introduction

1.1. Applications of cryogenic fluids

Cryogenic fluids are prevalent in a broad range of daily applications. For example, Liquid Nitrogen (LN_2) is used to flash freeze food, preserve tissues and blood, and destroy unhealthy tissues in cryosurgery. Liquid Oxygen (LOX) is used in the medical industry, life support systems, and fuel cells, while Liquid Hydrogen (LH_2) is used to cool superconducting magnets.

Cryogens, especially LOX, LH_2, Liquid Methane (LCH_4), and Liquid Helium (LHe), are also vitally important to space applications, the primary focus of the present study. Liquid Helium (LHe), for example, is used to chill down Earth-orbiting telescopes and satellites as well as cool space experiments. LOX/LCH_4 or LOX/LH_2 are used in ascent stages, descent stages, and in-space fuel depots, while LH_2 will also be used for nuclear thermal propulsion systems. LH_2 has also been proposed for use in several other advanced propulsion systems, both as propellent and coolant. Fig. 1(a) shows examples of space applications of cryogens.

1.2. Fluid physics unique to cryogens

Cryogens constitute a unique class of fluids which are clearly distinguishable from water and refrigerants by virtue of their

* Correspondence author at: Purdue University Boiling and Two-Phase Flow Laboratory (PU-BTPFL), School of Mechanical Engineering, Purdue University, 585 Purdue Mall, West Lafayette, IN 47907, U.S.A.
E-mail address: mudawar@ecn.purdue.edu (I. Mudawar).

https://doi.org/10.1016/j.ijheatmasstransfer.2022.122579
0017-9310/

Nomenclature

A_g	surface area occupied by vapor jets in single cell
A_w	total surface area of cell
b	ratio of wetting front length to critical wavelength in Interfacial Lift-off Model
C_{CHF}	function of surface orientation
c_p	specific heat at constant pressure
d	diameter of heated disc
D_j	diameter of vapor jet perpendicular to and away from heating surface
F_{sub}	subcooling function
g	gravitational acceleration
g_0	parameter in CHF correlation
H	height of vertical ribbon; thickness of heating wall
H'	dimensionless height of vertical ribbon
h_{fg}	latent heat of vaporization
K	dimensionless CHF; empirical coefficient
k	thermal conductivity; parameter in CHF correlations
k_w	thermal conductivity of heating wall
MAE	mean absolute error
N	number of data points
P	pressure
P_R	reduced pressure, P/P_{crit}
Pr	Prandtl number
q''	heat flux from heating wall
q''_{CHF}	critical heat flux (CHF)
R_a	arithmetic mean of surface roughness
R_i	gas constant
RMS	root mean squared error
S	thermal conductivity parameter of the wall, $H\sqrt{(\rho c_p k)_w}$
S_m	mean spacing between surface roughness peaks
S_c	subcooling parameter
T	temperature
T_f	bulk liquid temperature
T_{sat}	saturation temperature
T_w	wall temperature
ΔT_{sub}	liquid subcooling, T_{sat} - T_f
u_f	liquid velocity perpendicular to and toward heating wall
u_g	vapor velocity perpendicular to and away from heating wall
y	coordinate perpendicular to and away from heating wall

Greek Symbols

α	contact angle; thermal diffusivity
δ	liquid macro-layer thickness in Macrolayer Dryout Model; mean thickness of vapor layer in Interfacial Lift-off Model
λ_C	critical wavelength
λ_d	Taylor most dangerous wavelength
λ_H	critical Helmholtz wavelength
λ_T	Taylor wavelength
μ	dynamic viscosity
ν	specific volume
ρ	density
σ	surface tension
τ	time function in Zuber's subcooled CHF model
θ	angle of inclination from horizontal plane; percentage of data points predicted within ±30%
ξ	percentage of data points predicted within ±50%

Subscripts

CHF	corresponding to critical heat flux
crit	critical point
exp	experimental (measured)
f	saturated liquid
g	saturated vapor
h	high-pressure correlation
l	low-pressure correlation
pred	predicted
sat	saturated condition
sub	subcooled condition
w	heating wall
Zuber	based on Zuber model

low saturation temperatures (calculated using REFPROP 10 [2]) as shown in Fig. 1(b).

Fig. 2(a) compares saturated liquid properties for coolants belonging to the different classes, namely density, ρ_f, specific heat at constant pressure, $c_{p,f}$, thermal conductivity, k_f, viscosity, μ_f, and Prandtl number, Pr_f, each plotted against reduced pressure, P_R, ranging from 0 to 1. These plots highlight important differences between cryogens and other liquid classes (albeit with some exceptions), such as low ρ_f, high $c_{p,f}$, and low μ_f, with LHe showing the most extreme deviations even among the cryogens.

Low saturation temperatures for cryogens imply these fluids are highly susceptible to phase change in most space applications Fig. 2.(b) compares variations of relevant phase change properties for cryogens, namely vapor density, ρ_g, latent heat of vaporization, h_{fg}, and surface tension, σ, with P_R compared to those of other fluid classes. Here too, with some exceptions, cryogens display obvious property deviations, especially low ρ_g and σ, with LHe exhibiting the most deviations.

The unique thermophysical properties of cryogens pose appreciable challenges when conducting experimental temperature measurements. This particularly is the case for values of wall superheat, $T_w - T_{sat}$, or wall-to-fluid temperature difference, $T_w - T_f$, approaching or below 0.5 K, which is more commonly encountered with cryogens than with water or refrigerants. In these situations, heat transfer coefficient data might exhibit erroneous trends in the form of large artificial spikes or even unphysical values below zero. Two important inferences regarding the temperature measurement challenges are: (a) investigators should always be mindful of the potential for high uncertainties when interpreting cryogen data, and (b) these high uncertainties create appreciable scatter when aiming to develop correlations from experimental cryogen data.

1.3. Pool boiling heat transfer

Aside from being the simplest and most cost effective of all two-phase cooling schemes, pool boiling is the most prevalent and most mature in industry and is found in both low temperature and high temperature applications. Examples of the former include cooling of electronic components, power devices, and superconductor coils, where pool boiling capitalizes upon the coolant's latent heat to remove large amounts of heat while maintaining device temperatures safely below material and reliability limits. A prime example of high temperature applications is quenching of metal alloy parts in pursuit of optimum alloy microstructure and superior mechanical properties.

1.3.1. Measurement and characterization of pool boiling heat transfer: boiling curve versus quench curve

Pool boiling heat transfer mechanisms and regimes are commonly described with the aid of a *boiling curve* which is generally

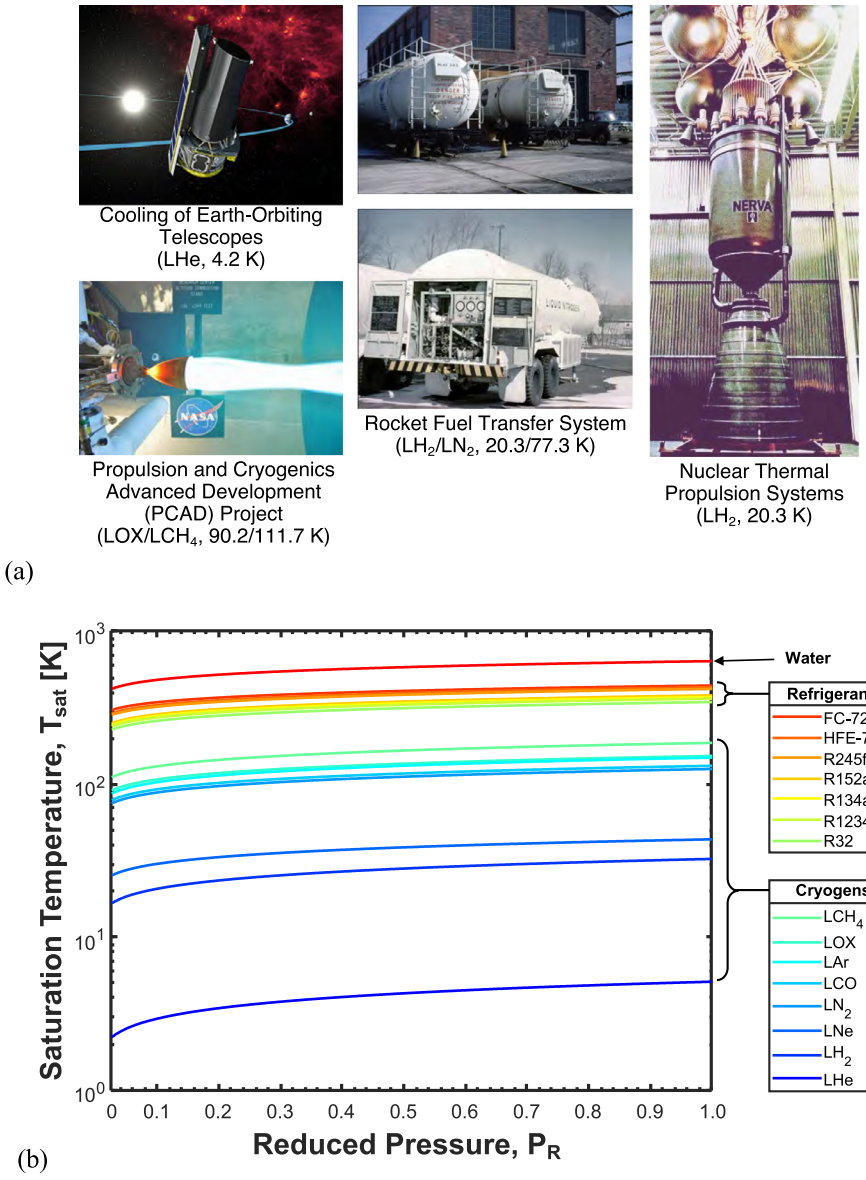

Fig. 1. (a) Examples of space applications of cryogens. (b) Classification of coolants into water, refrigerants, and cryogens based on variation of saturation temperature with reduced pressure. Adapted from Ganesan *et al.* [1].

measured using the *steady-state heating method*, or a *temperature-time curve* obtained using the *transient (quench) method*. Overall, the steady-state heating method is preferred in pool boiling studies because of its far greater accuracy in measuring heat transfer parameters of interest.

Shown in Fig. 3(a), using the steady-state heating method, a boiling curve is generated by initiating tests at zero power and increasing or decreasing wall heat flux in small increments, followed each by an adequate waiting period to allow wall temperature to reach steady state before it is measured. This method is typically implemented in two steps. First, the wall heat flux is increased in small increments to capture the *single-phase liquid regime, point of incipient boiling* (also termed *onset of boiling, ONB), nucleate boiling regime, critical heat flux (CHF) point,* and upper portion of the *film boiling region* (following the CHF wall temperature excursion). In the second step, starting at the film boiling condition reached at the end of the first step, the wall heat flux is decreased in small increments to capture the lower portion of the *film boiling region* and *minimum heat flux (MHF) point*, before triggering a sudden decrease in wall temperature toward the *nucleate boiling regime,* followed by the *ONB point*, and finally the *single-phase liquid regime*. Lacking from both steps of the steady state method is ability to capture the *transition boiling regime* of the boiling curve.

The second measurement method relies on initial preheating of the wall to a temperature well within *film boiling*, followed by *quenching* in liquid. A complete temperature-time (quench) curve is generated, Fig. 3(b), capturing all boiling regimes and transition points. Notice that the shape of the quench curve is highly dependent on thermal mass of the wall. Eventually, variation of the heat flux with wall superheat for each regime is determined via transient conduction analysis of the wall, generally using a lumped mass model.

1.3.2. Pool boiling critical heat flux (CHF)

CHF is arguably the most important design and safety parameter for most heat flux controlled boiling systems. This is because exceeding CHF will trigger a rapid and unsteady transition from highly efficient nucleate boiling to very heat transfer deficient film boiling. This transition is manifest by a sharp increase in surface temperature that may lead to physical damage, meltdown, or

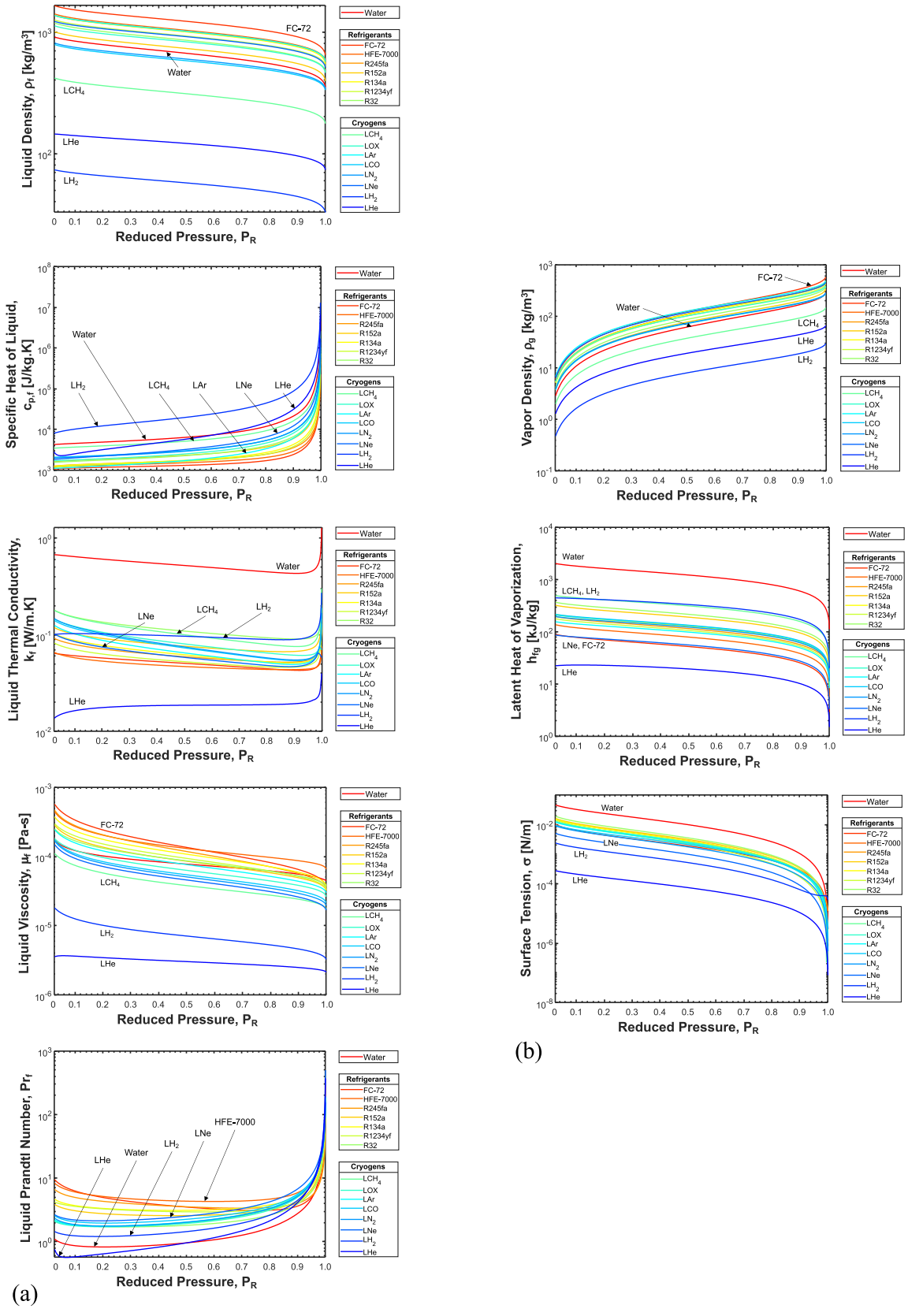

Fig. 2. (a) Variations of saturated liquid properties (density, specific heat at constant pressure, thermal conductivity, viscosity, Prandtl number) with reduced pressure. (b) Variations of saturated vapor density, latent heat of vaporization, and surface tension with reduced pressure.

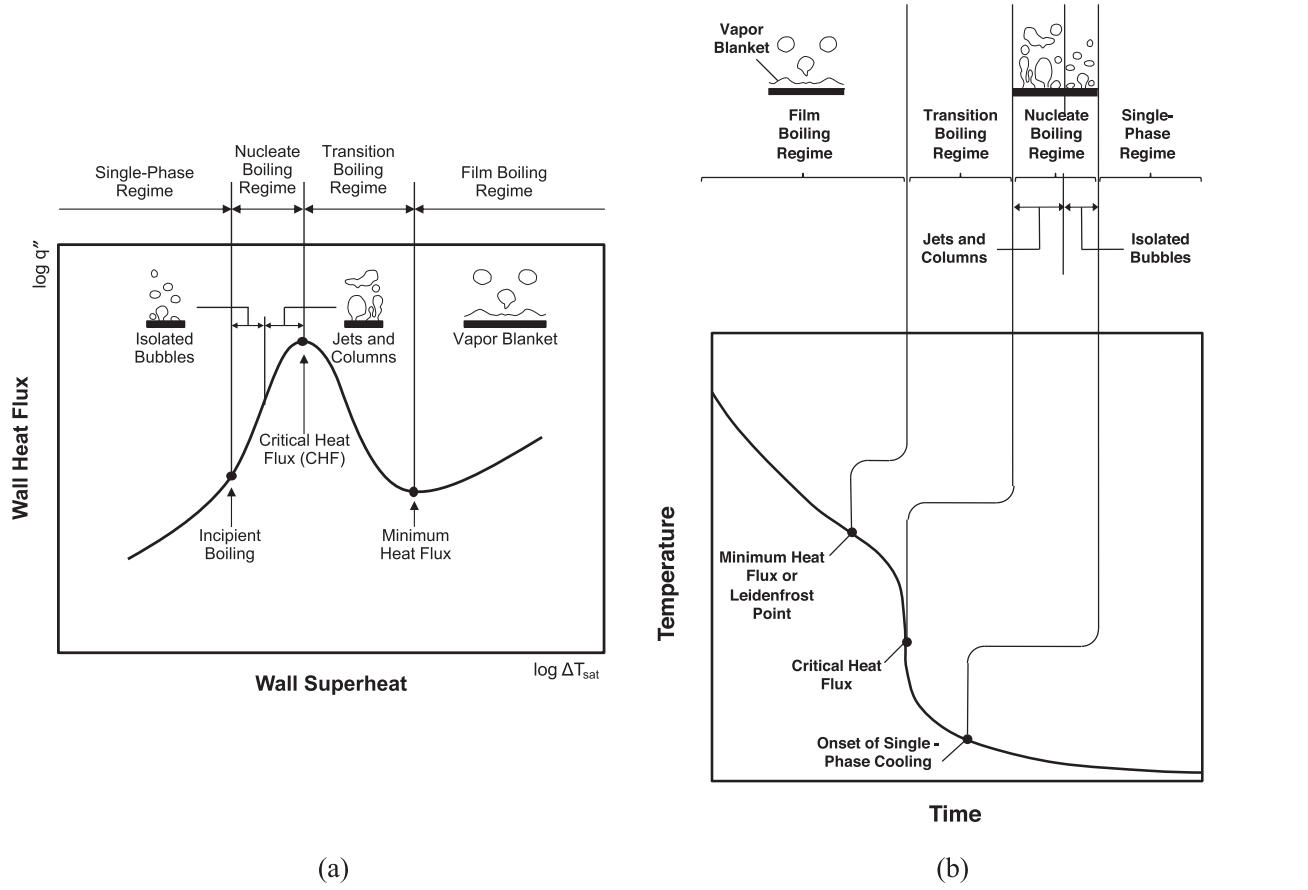

Fig. 3. (a) Pool boiling curve, generally measured using the steady-state heating method. (b) Pool quench curve, generally measured using the transient (quench) method.

burnout of the surface, which explains why CHF occurrence is often referred to as 'boiling crisis'. From a practical point of view, optimum cooling is achieved by maintaining conditions within the nucleate boiling regime, above the onset of boiling, but safely below CHF. Given the great importance of CHF to the design of cooling systems, investigators have studied its mechanisms for decades in pursuit of predictive models and/or experimental correlations.

By comparing how pool boiling CHF is measured using the heating method, Fig. 3(a), versus the quenching method, Fig. 3(b), it is obvious measurement accuracy is highly compromised for the latter. Using quenching data, CHF corresponds to the inflection point in the temperature-time plot, which is difficult to ascertain and often associated with high uncertainty in detecting corresponding wall temperature. This fact points to two important inferences regarding CHF measurement:

(1) When amassing data for pool boiling CHF in cryogenic fluids from literature, it is vitally important to segregate data obtained using the heating versus quenching methods.
(2) Developing a new universal model or correlation for pool boiling CHF in cryogenic fluids should be based on the more reliable and accurate heating data alone.

1.4. Objectives of present study

The proposed study concerns technologies related to cryogenic propellant production, storage, transfer, and usage to support the National Aeronautics and Space Administration's (NASA's) *in-situ* resource utilization (ISRU) goals. They include a broad range of applications, scales, and environments consistent with future NASA missions to the Moon and Mars.

More specifically, the study is part of a long-term effort to develop a piecewise-smooth set of correlations for use in lumped node codes to facilitate prediction of the entire pool boiling curve associated with cryogenic storage and transfer systems. This includes development of sub-models for all regimes and transition points of the boiling curve. The present study is focused entirely on developing an improved correlation for CHF.

Key objectives of this study are as follows:

(1) Review available pool boiling CHF models and correlations.
(2) Amass from World literature a consolidated database for pool boiling CHF for LHe, LH_2, LAr, LN_2, LO_2, and LCH_4.
(3) Assess the accuracy of availability models and correlations against the consolidated database.
(4) Explore parametric trends important to implementing models and correlations in NASA's cryogenic propellant production, storage, transfer, and usage. They include effects of (a) pressure, (b) subcooling, (c) heating surface orientation, (d) surface size, thickness, thermal properties, and surface finish, (e) contact angle, and (f) body force (microgravity, Earth gravity, Lunar gravity, Martian gravity).
(5) Propose a new universal correlation capable of tackling the unique properties of cryogens (*e.g.,* low saturation temperature, low latent heat of vaporization, low surface tension, *etc.*), with the ultimate goal of achieving improved predictive accuracy.

2. Prior pool boiling CHF models and correlations

2.1. CHF trigger mechanisms

Predicting CHF has been a primary goal for investigations at the Purdue University Boiling and Two-phase Flow Laboratory (PU-

BTPFL) since the mid-1980s. These efforts encompassed virtually all boiling schemes, including capillary [3], pool boiling [4], falling film [5], macro-channel flow boiling [6], micro-channel flow boiling [7,8], spray cooling [9], jet impingement cooling [10,11], and hybrid combinations of the different schemes [12]. With exception of capillary and spray cooling schemes, these studies revealed certain similarities in the CHF 'trigger' mechanism but also differences, stemming mostly from details of the bulk liquid flow.

For pool boiling, five different CHF mechanisms are prevalent in the literature: Rohsenow and Griffith's *Bubble Interference* [13], Zuber's *Hydrodynamic Instability* [14], Haramura and Katto's, *Macrolayer Dryout* [15], *Hot/Dry Spot* by Theofanous and Dinh [16] and Yagov [17], and Mudawar et al.'s *Interfacial Lift-off* [18]. Among the five mechanisms, Zuber's theory of hydrodynamic instability has attracted the most attention, being the first theoretical and mechanistic CHF model. In fact, a majority of published pool boiling CHF studies consist of efforts to improve predictive capability of the Zuber model by accounting for parametric effects not captured in the original model. Since these mechanisms have been thoroughly reviewed in a recent article by Liang and Mudawar [19] (for different fluids and not cryogens in particular), only a brief summary is provided below.

Before highlighting the different CHF mechanisms, it is important to mention an early pioneering investigation that led to the popular CHF formulation adopted later by many investigators. In 1948, Kutateladze [20,21] addressed pool boiling CHF by identifying dominant parameters governing momentum of vapor release from the wall, buoyancy, and surface tension. Using dimensional analysis, he arrived at the well-known relation

$$\frac{q''_{CHF}}{\rho_g h_{fg}\left[\sigma g\left(\rho_f-\rho_g\right)/\rho_g^2\right]^{1/4}} = K, \tag{1}$$

where K is a constant referred to hereafter as dimensionless CHF. The value of $K = 0.16$ was recommended by Kutateladze for pool boiling from large horizontal flat surfaces based on prior empirical data.

In one of the earliest investigations of pool boiling CHF, Rohsenow and Griffith [13] postulated that CHF would commence when initially isolated spherical vapor bubbles begin touching one another in tight formation before departure, Fig. 4(a), causing them to coalesce radially into a continuous insulating vapor layer.

Inspired by Kutateladze's formulation, Zuber [14] constructed a model for CHF in saturated pool boiling on an infinite flat surface based on hydrodynamic instability theory. A follow-up study by Zuber et al [22]. provided further details of the original model. As indicated in Fig. 4(b), just prior to CHF occurrence, vapor columns or jets were postulated to emanate at mean velocity u_g perpendicular to and away from the surface, as the surface is being replenished by liquid flowing between the jets and towards the surface at velocity u_f. The surface was modeled as consisting of repeated square cells, each consisting of a single jet and surrounding liquid. Zuber further assumed that the vapor jets, of diameter D_j, are formed along the surface by Taylor instability such that $D_j = 0.50\ \lambda_T$, where λ_T is the Taylor wavelength whose value is between the 'critical' wavelength corresponding to onset of instability, and 'most dangerous wavelength' corresponding to fastest growth of instability. The next crucial step of the model concerns the *trigger mechanism* for CHF. Because of velocity differences between the vapor and liquid, the interface of the vapor jet incurs Helmholtz instability with wavelength λ_H, growth of which causes merging of adjacent vapor jets, Fig. 4(b), giving rise to formation of the 'vapor mushroom' responsible for preventing bulk liquid from replenishing the surface.

Citing previous visualization results for vapor structures in pool boiling, Haramura and Katto [15] attributed pool boiling CHF to intermittent behavior of coalescent vapor bubbles and consumption of a liquid macrolayer beneath the coalescent bubbles; key foundations of their Macrolayer Dryout Model. Illustrated schematically in Fig. 4(c), Helmholtz instability in a large number of vapor stems emanating across the liquid macrolayer culminates in a large hovering bubble. They suggested growth of the large bubble is the result of consumption of the macrolayer by evaporation, and CHF will occur when the liquid macrolayer dries out just before departure of the large bubble.

The Hot/Dry Spot Model is based on the hypothesis that pool boiling CHF is the outcome of numerous small dry spots forming on the heating surface during nucleate boiling. Theofanous and Dinh [16] proposed CHF is governed by dynamics and instability of the liquid sublayer beneath large bubbles, leading to irreversible growth of the hot spots. In a different formulation, Yagov [17] hypothesized the evaporating liquid macrolayer trapped beneath each large coalescent vapor bubble is replenished by radial liquid inflow from the thicker, outer part of the microlayer, and CHF will occur when the liquid replenishing the boundary of the dry spot is completely evaporated, precipitating eventual unsteady growth of the dry spot.

The Interfacial Lift-off Model was originally developed by Galloway and Mudawar [23,24] based on extensive high-speed video motion analysis of interfacial behavior in flow boiling. Later, Mudawar et al [18]. and Howard and Mudawar [25] found the interfacial behavior at CHF in pool boiling along inclined and vertical surfaces to bear close resemblance to flow boiling CHF. They proposed a series of events that culminate in CHF. At heat fluxes slightly below CHF, intense vapor production results in a vapor layer that propagates along the surface. Helmholtz instability produces pronounced waves in this layer, permitting liquid contact with the surface only in 'wetting fronts' corresponding to the wave troughs, as depicted in Fig. 4(d). These wetting fronts sweep along the surface, providing the last source of surface cooling just prior to CHF. The trigger mechanism for CHF was described as lifting of the most upstream wetting front from the heating wall, which occurs when intense vapor momentum in the wetting front perpendicular to the wall begins to exceed the opposing pressure force resulting from interfacial curvature, Fig. 4(d). Using data from several sources, Howard and Mudawar showed that orientations effects on CHF for $0 < \theta < 90°$ are very weak, meaning their theoretical formulation for $\theta = 90°$ is equally valid for $\theta = 0°$.

2.2. Other models and correlations

There have been numerous investigations taking advantage of essentially the same CHF mechanisms of the afore-mentioned models to account for effects other than those for which the original models were developed; a detailed summary is provided in a later section. The popularity of Zuber's Hydrodynamic Instability Model [14] is clearly manifest by the largest number of works relying on essentially the same CHF mechanism to account for such effects as wall orientation, size, material, and surface roughness, as well as contact angle. Similarly, there have been several attempts to improve predictive accuracy of Haramura and Katto's Macrolayer Dryout Model [15] and Mudawar *et al.*'s Interfacial Lift-off Model [18].

Since a primary goal of the present study is to assess predictive accuracy of prior CHF predictive tools against cryogen data, a systematic strategy is adopted in which individual models and correlations are assessed only with respect to the parameters they are intended for by original authors. Details of this strategy will be explained later after describing the process of amassing cryogen data for the assessment study.

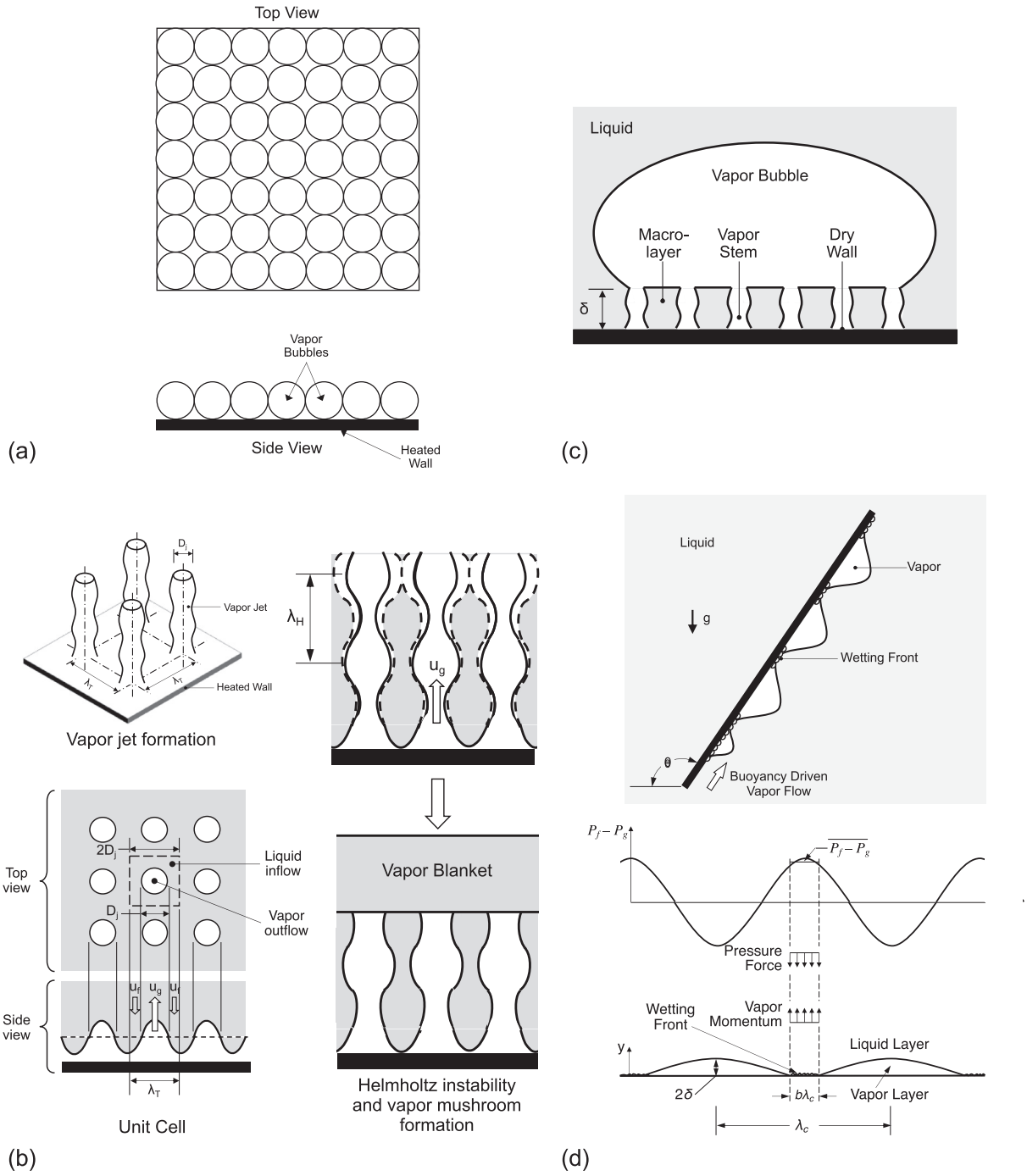

Fig. 4. Schematics of pool boiling CHF models: (a) Rohsenow and Griffith's Bubble Interference [13], (b) Zuber's Hydrodynamic Instability [14,22], (c) Haramura and Katto's Macrolayer Dryout [15], and (d) Mudawar *et al.*'s Interfacial Lift-off [18].

3. New consolidated cryogenic pool boiling CHF database

3.1. Compilation of CHF data and application of exclusion criteria

In the present study, references and data are compiled from world literature through a comprehensive data mining effort following closely a method recently adopted by Ganesan et al [26]. in compiling cryogen flow boiling CHF data. The majority of references for the present pool boiling CHF data are from Advances in Cryogenic Engineering (Springer publication) and Cryogenics (Elsevier publication). Apart from those two sources, data are also obtained from NASA Technical Notes, other journal papers, conference papers, and theses from across the globe.

CHF data are extracted from the literature using one of two methods: (a) digitization from data plots using WebPlotDigitizer software [27], or (b) direct extraction from tables. The CHF datapoints are identified in one of three forms: (1) explicitly indicated as CHF data, (2) peak nucleate boiling heat flux data from boiling curves, or (3) plots of normalized CHF in reduced gravity versus normalized gravitational acceleration. There were difficulties acquiring data from specific sources, which required cross-referencing with other sources. For example, heat flux versus wall superheat plots by Garcia [28] are available without scale due

to a confidentiality clause in their study. Hence, a scale for the same data was obtained from another study by Wang *et al.* [29]. Similarly, heated surface dimensions and orientation information missing from a NASA Technical Memorandum by Graham *et al.* [30] were obtained from another reference by Baldwin *et al.* [31].

Various complications arose while acquiring references for the data mining effort such as (1) unavailability of references from Purdue University's Interlibrary Loan (ILL), (2) reluctance of a few investigators to share their own data, and (3) duplicate data. Data duplication was avoided by a point-by-point inspection of CHF data from different sources.

Additionally, since the main focus of this study is CHF from flat surfaces, data obtained from experiments employing wire, tube, cylinder, or narrow rectangular channel as heating element are excluded from consideration. After the initial effort of excluding duplicate data, focus shifted toward further exclusion of data that do not satisfy the following requirements:

(1) Only pure cryogenic fluids; data for fluid mixtures are excluded.
(2) Pool boiling on uniformly heated flat surfaces, including those both 'infinite' and finite.
(3) Steady-state pool boiling; quench data are excluded due to large and rapid variations in wall temperature at CHF.
(4) Subcritical pressure and temperature, including both saturated and subcooled conditions.
(5) All orientation angles.
(6) Gravitational accelerations only from 0 to 1 *g*.
(7) Unmodified as well as roughened heating surfaces; finned or coated surfaces are excluded.
(8) Data with all information necessary for correlating data (*e.g.*, operating pressure, heat flux, pool (bulk) temperature, surface orientation angle, gravitational acceleration, *etc.*).

Detailed information regarding data exclusions is provided in Table 1.

Additional Physics-based data exclusion strategies are applied to the compiled database in addition to the exclusion strategies described above. They include data for 'superfluid' helium (He II), which possesses physical behavior and thermophysical properties vastly different from those of He I and other cryogenic fluids, including zero viscosity and zero entropy. For example, Hata et al [72]. investigated effects of subcooling and surface orientation on pool boiling CHF for helium, and some experiments showed a vanishing effect of orientation for bulk temperatures below the Lambda Temperature (2.17 K) corresponding to He II. The CHF data belonging to this temperature range are excluded from the consolidated database because corresponding complex and unique physical behavior is beyond the scope of the present study. Also excluded are any supercritical data. These consist not only of bulk fluid temperatures and pressures that exceed the critical point, but also wall temperatures that exceed the critical temperature. This criterion resulted in exclusion of 24 data points from the consolidated database. Details concerning the physics-based data exclusions are provided in Table 2.

It is important to note that additional data exclusions are adopted later based on other criteria that will be discussed after initial assessment of previous models and correlations.

3.2. Consolidated cryogenic pool boiling CHF database

The Consolidated Cryogenic Pool Boiling CHF Database (termed Consolidated Database hereafter) that will be used for assessment of prior CHF models and correlations is the outcome of application of all the afore-mentioned data exclusion strategies. Details of the Consolidated Database, including author(s) (reference), number of acceptable data points, heater geometry, heater size, heater material, surface roughness or treatment, operating pressure, inclination angle, and boiling state, are detailed in Table 3. It is comprised of a total of 1273 pool boiling CHF data points from 55 sources corresponding to six fluids: liquid Helium (LHe), liquid nitrogen (LN_2), liquid hydrogen (LH_2), liquid oxygen (LO_2), liquid Argon (LAr), and liquid methane (LCH_4), with a distribution of 39.51%, 32.36%, 9.66%, 13.83%, 3.38% and 1.26%, respectively. Additionally, 71.01% of the datapoints are for the horizontal upward facing orientation ($\theta = 0°$) and remaining 28.99% covering orientation angles between 15°and 360°. For simplicity and use of data with orientation angles that are both greater than 180° and associated with upward-facing surfaces in correlation assessment, orientation angles are converted to between 0° and 180° by simply subtracting from 360°. Finally, the Consolidated Database consists of reduced pressures ranging from 0.0037 to 0.9890.

The Consolidated Database is carefully segregated to assess predictive accuracy of individual CHF models and correlations based on applicability range for each. This is because different models and correlations are intended by original authors to incorporate effects of only a subset of parameters. The Consolidated Database is segregated according to both cryogen and parameters. This resulted in 10 cases, details for which are provided in Table 4.

4. Assessment of predictive accuracy of models and correlations

4.1. Statistical assessment parameters

The Consolidated Database is used to assess predictive accuracy of all reviewed models and correlations, details of which are provided in Table 5. Several statistical parameters are adopted in the assessment: mean absolute error (MAE), root mean square error (RMS), and percentage of data points predicted within ±30% (θ) and ±50% (ξ). Thermophysical properties of fluids at different pressures and temperatures are obtained using REFPROP 10 [81]. MAE and RMS are defined, respectively, as

$$MAE = \frac{1}{N}\sum \frac{\left|q''_{CHF,pred} - q''_{CHF,exp}\right|}{q''_{CHF,exp}} \times 100\% \tag{2}$$

$$\text{and } RMS = \sqrt{\frac{1}{N}\sum \left(\frac{q''_{CHF,pred} - q''_{CHF,\exp}}{q''_{CHF,\exp}}\right)^2} \times 100\%. \tag{3}$$

4.2. Models and correlations assessed using majority of datapoints in consolidated database, also used for developing new CHF correlation

4.2.1. Baseline models and correlations (Case 1)

For the baseline case (Case 1), 792 CHF datapoints for 6 cryogens from the Consolidated Database are used to assess accuracy of 18 models and correlations. Figs. 5 and 6 show a comparison of measured and predicted CHF for each model or correlation, while Table 6 provides a summary of corresponding statistical results. Overall, MAE values are quite close for several models and correlation. With nearly identical MAE values of 33.95%, 33.52%, 33.71% and 33.48%, the models and correlations of Zuber and Tribus [104], Lienhard and Dhir [108,109], Mudawar et al [18]. and Yagov [17], respectively, show best overall accuracy. Others providing fairly good results are those of Kutateladze [20], Zuber et al [14,22]., Chang and Snyder [105], Chang [106], Moissis and Berenson [107], Haramura and Katto [15], Bailey et al [114]., Soziev and Khrizolitova [110], Borishanskii [103] and Wang et al [29]., with MAEs of 35.15%, 34.71%, 36.78%, 34.91%, 35.32%, 35.05%, 38.27%, 36.51%, 43.63% and 34.26%, respectively. On the other hand, those by Rohsenow and Griffith [13], Sakashita and Ono [111] (using Kumada's macrolayer

Table 1
Summary of CHF data points excluded from consolidated database.

Refs.	Number of excluded data points	Data unidentifiable from plots	Duplicate data	Remarks
Class *et al.* [32]	5			• Only range of operating pressure provided for certain data points • Data for greased heat transfer surface
Kosky [33]	62		•	• Repetitive data from Lyon *et al.* [34]
Lyon *et al.* [34]	6			• Pseudocritical CHF data, obtained by rapid increase of power to test element
Graham *et al.* [30]	8	•		• Data points difficult to extract from plots • Data for acceleration > 1 g • Data for supercritical pressure • Pool temperature is missing
Lyon *et al.* [35]	13			• Data for acceleration < 0 g
Lyon [36]	7			• Erroneous data due to large step power increase • CHF data for superfluid helium
Cummings and Smith [37]	4			• Data for tin coated heat transfer surfaces
Kosky [38]	69			• Data for mixture of cryogenic fluids • Data from transient pool boiling experiments • Data inconsistencies due to use of fiber-glass insulation between test element and guard heater
Kosky and Lyon [39]	43		•	• Repetitive data from Kosky [38]
Lyon [40]	117		•	• Repetitive data from Kosky and Lyon [39] and Lyon [36] • CHF data for superfluid helium
Marto *et al.* [41]	7			• Data for Teflon coated heat transfer surface • Data for greased heat transfer surface • Data for modified surface by drilling cavities
Butler *et al.* [42]	30			• Data for variously treated surfaces to enhance heat transfer
Johannes [43]	9			• Missing experimental apparatus information • Data for pool boiling in a rectangular channel
Porchey *et al.* [44]	28		•	• Repetitive data from Porchey [45] • Data for oxidized heat transfer surface
Merte *et al.* [46]	12		•	• Repetitive data from Merte [47]
Jergel and Stevenson [48]	6		•	• Repetitive data from Jergel and Stevenson [49,50]
Ackermann *et al.* [51]	79			• Data for liquid nitrogen and liquid methane mixture
Warner and Park [52]	1	•		• Data points difficult to extract due to overlapping symbols
Grigoriev *et al.* [53]	5		•	• Repetitive data from Grigoriev *et al.* [54]
Kobayashi *et al.* [55]	94			• Data for pool boiling in a narrow rectangular channel • Data for superfluid helium
Ogata and Nakayama [56]	3			• Data for centrifugal acceleration > 1 g
Ogata and Nakayama [57]	18			• Data for variously treated (by creating different types of grooves) heat transfer surface • Data for oxidized heat transfer surface
Kirichenko *et al.* [58]	52			• Data for pool boiling in a rectangular channel
Chen and Van Sciver [59]	50			• Data for pool boiling in a rectangular channel
Jager *et al.* [60]	16			• Data for highly oxidized heat transfer surface
Beduz *et al.* [61]	40	•		• Data for different surfaces indistinguishable due to lack of information • Data for modified (plasma sprayed and grooved and rolled) heated surface to enhance heat transfer
Chandratilleke *et al.* [62]	11			• Data for Polytetrafluoroethylene (PTFE) coated heat transfer surface
Ashworth *et al.* [63]	21			• Data for porous heated surface produced by plasma spraying to enhance heat transfer
Ogata and Mori [64]	6			• Data for variously coated heat transfer surfaces
Iwamoto *et al.* [65]	28			• Data for pool boiling in a rectangular channel
Scurlock [66]	13		•	• Repetitive data from Ashworth *et al.* [63] • Data for coated heat transfer surface
Drach and Fricke [67]	1			• Data for varnish coated heat transfer surface
Huang and Van Sciver [68]	15			• Data for pool boiling in a rectangular channel
Iwamoto *et al.* [69]	92			• Data for partially and completely oxidized heat transfer surface
Nguyen *et al.* [70]	28			• Data for pool boiling in a rectangular channel
Tatsumoto *et al.* [71]	47			• Data for superfluid helium
Hata *et al.* [72]	104	•		• Data points difficult to extract due to overlapping symbols • Data for oxidized heat transfer surface
Ohira and Furumoto [73]	6			• Data for slush nitrogen and slush hydrogen
Delov *et al.* [74]	5		•	• Repetitive data from Balakin *et al.* [75]
Total of excluded data points	**1161**			

Table 2
Summary of data points excluded from individual CHF databases.

Refs.	Total CHF data points	Critical condition $T_w > T_{crit}$	Acceptable CHF data points
Liquid Helium			
Cummings and Smith [37]	14	7	7
Jergel and Stevenson [50]	3	2	1
Ibrahim *et al.* [76]	12	2	10
Chandratilleke *et al.* [62]	6	3	3
Liquid Hydrogen			
Kozlov and Nozdrin [77]	14	2	12
Shirai *et al.* [78]	36	1	35
Shirai *et al.* [79]	1	1	0
Graham *et al.* [34]	11	2	9
Liquid Nitrogen			
Porchey [45]	66	3	63
Liquid Oxygen			
Lyon *et al.* [34]	25	1	24
Total	**188**	**24**	**164**

Table 3
Summary of consolidated database for flat surfaces.

Reference	Acceptable CHF data points	Heater geometry	Heater Size: Width x length [mm^2] or diameter (thickness) [mm]	Heater Material	Surface roughness [μm]	Pressure [MPa]	Inclination angle	Boiling State
Liquid Helium								
Lyon [36]	62	Circular	9.91 (8)	Platinum	Polished (with 400 grit carbide abrasive paper)	0.0061–0.2171	0°, 45°, 67.5°, 90°, 112.5°, 135°, 157.5°, 180°, 225°, 270°, 315°, 360°	Saturated
Cummings and Smith [37]	7	Circular	15.24 (50)	Copper [99.9%]	Mirror finish, grit ground, grit lapped	0.1013	0°	Saturated
Butler *et al.* [42]	3	Rectangular	50 × 10 (5)	Copper	Untreated, acetone cleaned, sandblasted	0.1013	90°	Saturated
Jergel and Stevenson [49]	3	Circular	15 (10)	OFHC Copper	-	0.1013	0°, 90°, 180°	Saturated
Jergel and Stevenson [50]	1	Circular	15 (10)	Al 59 [99.999%]	-	0.1013	180°	Saturated
Jergel and Stevenson [48]	3	Circular	15 (10)	Al 69 [99.9999%]	-	0.1013	0°, 90°, 180°	Saturated
Bewilogua *et al.* [80]	107	Circular	24.98	Copper	0.2 (ground with F9 Emery cloth)	0.0064 – 0.2178	0°, 90°, 135°, 165°	Saturated
Grigoriev *et al.* [54]	5	Circular	8	Copper M-1, bronze 6.5-0.15, nickel H-1, brass πM-62, stainless steel X18H9T	-	0.1	0°	Saturated
Vishnev *et al.* [81]	14	Rectangular	96 × 10.4 (0.063)	Stainless steel	-	0.1013	0°, 30°, 45°, 60°, 90°, 120°, 150°, 180°	Saturated
Deev *et al.* [82]	45	Square	30 × 30	Copper (99.993%)	0.08 (polished) – 0.3	0.1 – 0.2258	0°, 90°	Saturated
Ogata and Nakayama [56]	1	Circular	6.1	Copper	Polished	0.101	0°	Saturated
Ibrahim *et al.* [76]	10	Circular	25.4 (31.75)	OFHC Copper	-	0.0983 – 0.1307	0°	Saturated, subcooled
Verkin *et al.* [83]	32	Circular	20	Copper	-	0.1 – 0.2	0°	Saturated, subcooled
Ogata and Nakayama [57]	1	Square	15 × 15	Copper	Smooth	0.1013	0°	Saturated
Chandratilleke *et al.* [62]	3	Circular	20 (30)	Copper	Polished	0.1013	0°, 90°, 175°	Saturated
Nishio and Chandratilleke [84]	9	Circular	20 (30)	Copper	0.027 – 4.35	0.1013	0°, 45°, 90°, 135°, 175°	Saturated
Ogata and Mori [64]	2	Square	15 × 15	Copper	Untreated	0.1013	0°, 90°	Saturated
Iwamoto *et al.* [65]	14	Rectangular	18 × 76 (7.5)	Copper	Polished (roughness less than 10)	0.1013	0°, 15°, 30°, 45°, 60°, 75°, 90°, 105°, 120°, 135°, 150°, 165°, 172.5°, 180°	Saturated

(*continued on next page*)

Table 3 (*continued*)

Reference	Acceptable CHF data points	Heater geometry	Heater Size: Width x length [mm^2] or diameter (thickness) [mm]	Heater Material	Surface roughness [μm]	Pressure [MPa]	Inclination angle	Boiling State
Iwamoto *et al.* [69]	20	Rectangular	18 × 76 (7.5)	Copper	Polished (roughness less than 10)	0.1013	0°, 15°, 30°, 45°, 60°, 75°, 90°, 105°, 120°, 135°, 150°, 165°, 172.5°, 180°	Saturated
Iwamoto *et al.* [85]	52	Rectangular	18 × 10 (7.5), 18 × 18 (7.5), 18 × 40 (7.5), 18 × 76 (7.5)	Copper	Polished [roughness less than 10]	0.1013	0°, 15°, 30°, 45°, 60°, 75°, 90°, 105°, 120°, 135°, 150°, 165°, 172.5°, 180°	Saturated
Hata *et al.* [72]	69	Rectangular	10 × 40 (0.1)	Manganin	Untreated	0.1013 – 0.13	0°, 90°, 135°, 180°	Saturated, subcooled
Grigoriev *et al.* [86]	5	Circular	8 (40)	Copper, brass	1, 5, 10	0.1013	0°	Saturated
Iwamoto *et al.* [87]	35	Rectangular	18 × 10 (7.5), 18 × 18 (7.5), 18 × 40 (7.5), 18 × 76 (7.5), 10 × 18 (7.5), 40 × 18 (7.5)	Copper	Polished (roughness less than 10)	0.1013	0°, 30°, 60°, 75°, 90°	Saturated
LHe CHF data	***503***							
Liquid Hydrogen								
Class *et al.* [32]	13	Rectangular	25.4 × 558.8 (0.127)	Karma alloy	0.15 (smooth), 0.67 (rough)	0.0831 – 0.8511	0°, 45°, 90°	Saturated
Graham *et al.*[a] [30]	9	Rectangular ribbon	-	Chromel – A	-	0.2930 – 0.6722	90°	Saturated, subcooled
Merte [47]	6	Circular	76.2	Copper	-	0.1023 – 0.1027	0°, 90°, 180°	Saturated
Bewilogua *et al.* [80]	31	Circular	19.22	Copper	0.2 (ground with F9 Emery cloth)	0.1036 - 1.2604	0°	Saturated
Kozlov and Nozdrin [77]	12	Circular	30 (8, 18, 12)	Stainless steel, Aluminum alloy, copper	-	0.0072 – 0.13	0°	Saturated
Ohira and Furumoto [73]	8	Circular	25	ETP Copper	Less than 1	0.00704-0.1013	0°, 90°, 180°	Saturated
Shirai *et al.* [78]	35	Rectangular	10 × 100 (0.1)	Manganin	-	0.11 – 1.0994	0°	Saturated, subcooled
Garcia[b] [28]	9	Circular	11.28	Copper	-	0.1 – 0.2	0°	Saturated, subcooled, acceleration ~ 0g, 0.1g, 1g
LH_2 CHF data	***123***							
Liquid Nitrogen								
Kosky[c] [33]	10	Flat ring	ID – 64.5 OD – 68.5 (0.0508)	Platinum	-	0.1986 - 0.4357	0°	Saturated
Lyon *et al.* [34]	31	Flat ring	ID – 64.5 OD – 68.5 (0.0508)	Platinum	-	0.0419 – 2.5382	0°	Saturated
Kosky [38]	142	Circular	19.05	Platinum	Polished	0.1019 - 3.3532	0°	Saturated
Lewis *et al.* [88]	2	Circular	76.2	Copper	-	0.0986 – 0.3054	90°	Saturated, subcooled
Marto *et al.* [41]	5	Circular	25.4 (21.08, 9.093)	ETP copper; nickel	Mirror finish; roughened;	0.1013	0°	Saturated
Merte[d] [47]	20	Circular	76.2	Copper	-	0.0986	0°, 90°, 180°	Saturated; gravity ~ 0.008g, 1g
Porchey [45]	63	Circular	38.1	Gold, silver	Chemically etched, mirror finish, electrolytically etched, electropolished	0.3392-3.053	0°	Saturated

(*continued on next page*)

Table 3 (*continued*)

Reference	Acceptable CHF data points	Heater geometry	Heater Size: Width x length [mm^2] or diameter (thickness) [mm]	Heater Material	Surface roughness [μm]	Pressure [MPa]	Inclination angle	Boiling State
Akhmedov *et al.* [89]	12	Circular	10	Cr18Ni9Ti steel, M-1 copper	-	0.1 – 3.2	0°	Saturated
Swanson and Bowman [90]	1	Circular	12.7	Sapphire	-	0.1013	0°	Saturated
Ackermann *et al.* [51]	3	Circular	19.22	Copper	0.2 (ground with F9 Emery cloth)	0.2 – 2.1	0°	Saturated
Bewilogua *et al.* [80]	26	Circular	24.98	Copper	0.2 (ground with F9 Emery cloth)	0.0983 – 3.037	0°	Saturated
Warner and Park [52]	7	Circular	38.1 (3.81)	Gold	-	0.0993	0°	Saturated
Ishigai *et al.* [91]	13	I -shaped	10, 20 (width)	Stainless steel	2, 3, rolled	0.1013	0°, 180°	Saturated
Nishio [92]	1	Circular	22 (60)	Oxygen free copper	-	0.1013	0°	Saturated
Beduz *et al.* [61]	2	Square	50 × 50 (6)	Aluminum, copper	Polished	0.1013	0°	Saturated
Ashworth *et al.*[e] [63]	1	Square	25.4 × 25.4 (5)	Aluminum	-	0.1013	90°	Saturated
Kirichenko *et al.* [93]	24	Circular, rectangular	22 (3.1), 20 (2), 29.5 × 8 (2), 29.7 × 8 (3.7)	HTS ceramic samples of YBa2Cu307	-	0.013-0.4503	0°	Saturated
Nguyen *et al.* [70]	7	Rectangular	20 × 10 (2.54)	Copper	-	0.1013	0°, 30°, 60°, 90°, 180°, 300°, 330°	Saturated
Ohira and Furumoto [73]	3	Circular	25	ETP copper	Less than 1	0.0125, 0.1013	0°	Saturated
Duluc *et al.* [94]	2	Circular	30	Copper	0.06 (mirror finish), 1 (rough)	0.1013	0°	Saturated
Jin *et al.* [95]	1	Square	60 × 60 (17.5)	Stainless steel (1Cr18Ni9Ti)	-	0.1	0°	Saturated
Wang *et al.* [96]	1	Circular	32	Copper	-	0.1013	0°	Saturated
Jin *et al.* (2011) [97]	25	Circular	9, 12, 15	Copper (99.9%), brass (Cu 60.5-63.5%, rest Zn), Aluminum alloy (Si 0.2-0.6%, Fe 0.35%, Mg 0.45-0.9%, rest Al)	Polished	0.1013	0°	Saturated
Balakin *et al.* [75]	5	Rectangular	(25-40) x 2.5	Ni – W tape	-	0.1013	0°, 30°, 45°, 60°, 90°	Saturated
Bombardieri and Manfletti [98]	3	Rectangular	46 × 51	Copper, Aluminum, Stainless steel	0.076, 0.141, 0.117	0.09815 [atmospheric]	0°	Saturated
Zoubir *et al.* [99]	1	Rectangular ribbon	100 × 4 (0.025)	Brass	-	0.1013	0°	Saturated
Shiotsu *et al.* [100]	1	Rectangular tape (ribbon)	80 × 3.2 (0.23)	Silver sheathed BiPbSrCaCuO	-	0.1013	90°	Saturated
LN_2 CHF data	***412***							
Liquid Oxygen								
Lyon *et al.* [34]	24	Flat ring	ID – 64.5 OD – 68.5 (0.0508)	Platinum	-	0.0228 – 4.8484	0°	Saturated
Lyon *et al.*[f] [35]	26	Circular	19.05	Platinum	Polished	0.1013	0°	Saturated; gravity ~ 0g – 1g
Kosky[g] [38]	125	Circular	19.05	Platinum	Polished	0.0226 - 4.9193	0°	Saturated
Ashworth *et al.*[e] [63]	1	Square	25.4 × 25.4 (5)	Aluminum	-	0.1013	90°	Saturated
LOX CHF data	***176***							
Liquid Argon								

(*continued on next page*)

Table 3 (*continued*)

Reference	Acceptable CHF data points	Heater geometry	Heater Size: Width x length [mm^2] or diameter (thickness) [mm]	Heater Material	Surface roughness [μm]	Pressure [MPa]	Inclination angle	Boiling State
Kosky [38]	42	Circular	19.05	Platinum	Polished	0.0755 - 4.6201	0°	Saturated
Ashworth *et al.*[e] [63]	1	Square	25.4 × 25.4 (5)	Aluminum	-	0.1013	90°	Saturated
LAr CHF data	***43***							
Liquid Methane								
Kosky [38]	13	Circular	19.05	Platinum	Polished	0.0347 - 4.1201	0°	Saturated
Ackermann *et al.* [51]	3	Circular	19.22	Copper	0.2 (ground with F9 Emery cloth)	0.2 – 2.1	0°	Saturated
LCH_4 CHF data	***16***							
Total	**1273**							

[a] Experimental apparatus information taken from Baldwin et al. [31].
[b] Reduced gravity produced using variable magnetic field; a scale for data presented by Garcia was adopted from Wang et al. [101].
[c] Preliminary data at low pressures for LN_2 were obtained on Harman's [102] original surface.
[d] Reduced gravity produced using drop tower experiments.
[e] Heater dimensions measured using scale in the heated surface figure.
[f] Reduced gravity produced using variable magnetic field; CHF data obtained from normalized plots of CHF versus vs relative acceleration.
[g] 46 data points are for 99.8% LO_2 + 0.2% LAr.

Table 4
Segregation of CHF data relative to individual parameters.

Case	Infinite	Saturated	Subcooled	Orientation	Contact angle	Conduction	Roughness	Finite
Models and correlations assessed using majority of datapoints in Consolidated Database, also used for developing new CHF correlation								
1	√	√						
2	√	√		√				
3	√	√	√					
4	√	√	√	√				
Correlations assessed using portions of Consolidated Database missing values for essential surface parameters								
5	√	√			√			
6	√	√		√	√			
7	√	√				√		
8	√	√	√			√		
9	√	√			√		√	
10	√	√						√

Table 5
Segregation of CHF models and correlations.

Author(s)	Model(s) or Correlation(s)
Case 1: saturated, 1g, infinite, horizontal	
Kutateladze [20]	$q''_{CHF} = 0.16\rho_g h_{fg}[\sigma g(\rho_f - \rho_g)/\rho_g^2]^{1/4}$
Rohsenow and Griffith [13]	$q''_{CHF} = 0.012\rho_g h_{fg}\left(\frac{\rho_f - \rho_g}{\rho_g}\right)^{0.6}$
Borishanskii [103]	$q''_{CHF} = \left[0.13 + 4\left\{\frac{\rho_f \sigma^{3/2}}{\mu_f^2[g(\rho_f - \rho_g)]^{1/2}}\right\}^{-2/5}\right] \times \rho_g h_{fg}[\sigma g(\rho_f - \rho_g)/\rho_g^2]^{1/4}$
Zuber *et al.* [14,22]	$q''_{CHF} = 0.131\rho_g h_{fg}[\sigma g(\rho_f - \rho_g)/\rho_g^2]^{1/4}$
Zuber and Tribus [104]	$q''_{CHF} = \frac{\pi}{24}\rho_g h_{fg}[\sigma g(\frac{\rho_f - \rho_g}{\rho_g^2})]^{1/4}[\frac{\rho_f}{\rho_f + \rho_g}]^{1/2}$
Chang and Snyder [105]	$q''_{CHF} = 0.145\rho_g h_{fg}[\sigma g(\rho_f - \rho_g)/\rho_g^2]^{1/4}\left[\frac{\rho_f + \rho_g}{\rho_f}\right]^{1/2}$
Chang [106]	$q''_{CHF} = 0.13\rho_g h_{fg}[\sigma g(\rho_f - \rho_g)/\rho_g^2]^{1/4}$
Moissis and Berenson [107]	$q''_{CHF} = 0.18\frac{\rho_g h_{fg}\left[\frac{\rho_f + \rho_g}{\rho_f \rho_g}\right]^{1/2}[gg_0\sigma(\rho_f - \rho_g)]^{1/4}}{1 + 2(\rho_g/\rho_f)^{1/2} + (\rho_g/\rho_f)}$

(*continued on next page*)

Table 5 (*continued*)

Author(s)	Model(s) or Correlation(s)
Lienhard and Dhir [108,109]	$q''_{CHF} = 0.149\rho_g h_{fg}[\sigma g(\rho_f - \rho_g)/\rho_g^2]^{1/4}$
Haramura and Katto [15]	$q''_{CHF} = K\left\{0.721\left(\frac{A_g}{A_w}\right)^{5/8}\left(1-\frac{A_g}{A_w}\right)^{5/16}\left[\left(\frac{\rho_f}{\rho_g}+1\right)/\left(\frac{11}{16}\frac{\rho_f}{\rho_g}+1\right)^{3/5}\right]^{5/16} \times \rho_g h_{fg}[\sigma(\rho_f-\rho_g)g/\rho_g^2]^{1/4}\right\}$ where $A_g/A_w = 0.0584(\rho_g/\rho_f)^{0.2}$ and $K = \begin{cases} 1 & \textit{for infinite surface} \\ \left[\left(\frac{\sqrt{3}\pi}{H'}\right)^{1/16}\left[1+\frac{1}{2}\left(\frac{\pi}{H'}\right)^2\right]^{1/32}\right] & \textit{for vertically oriented ribbons} \\ \left[(1+k)^{5/16}\left\{\left[3^{1/2}\cdot 2\pi\left(\frac{\sigma}{g(\rho_f-\rho_g)}\right)^{1/2}\right]^2/\left(\frac{\pi}{4}d^2\right)\right\}^{1/16}\right] & \textit{for small disk} \end{cases}$ where $H' = H/[\sigma/g(\rho_f-\rho_g)]^{1/2}$
Soziev and Khrizolitova [110]	$q''_{CHF} = 0.16\{1+[\sigma g(\rho_f-\rho_g)]^{1/2}/P\}^{1/2} \times \rho_g h_{fg}[\sigma g(\rho_f-\rho_g)/\rho_g^2]^{1/4}$
Sakashita and Ono [111,112]	$\frac{q''_{CHF}}{q''_{CHF,Zuber}} = 1.42\left(\frac{\rho_f}{\rho_g}\right)^{1/30}\left(1+\frac{\rho_g}{\rho_f}\right)^{1/3}$
Sakashita and Ono [111,113]	$\frac{q''_{CHF}}{q''_{CHF,Zuber}} = 4.98\left(\frac{\rho_f^3(\rho_f-\rho_g)g\nu_f^4}{\rho_g\sigma^3}\right)^{1/22}$
Mudawar *et al.* [18]	$q''_{CHF} = 0.151\rho_g h_{fg}[\sigma g(\rho_f-\rho_g)/\rho_g^2]^{1/4}$
Bailey *et al.* [114]	$q''_{CHF} = 0.1703\rho_g h_{fg}[\sigma g(\rho_f-\rho_g)/\rho_g^2]^{1/4}$
Gaun *et al.* [115]	$q''_{CHF} = 0.2445\left(1+\frac{\rho_g}{\rho_f}\right)^{1/4}\left(\frac{\rho_g}{\rho_f}\right)^{1/10}\rho_g h_{fg}[\sigma(\rho_f-\rho_g)g/\rho_g^2]^{1/4}$
Yagov [17]	$q''_{CHF,I} = 0.5\frac{h_{fg}^{81/55}\sigma^{9/11}\rho_g^{13/110}k_f^{7/110}g^{21/55}f(Pr_f)}{\nu_f^{1/2}c_{p,f}^{3/10}R_i^{79/110}T_{sat}^{21/22}}$ *for* $P/P_{crit} < 0.001$ here $f(Pr_f) = \left(\frac{Pr_f^{9/8}}{1+2Pr_f^{1/4}+0.6Pr_f^{19/24}}\right)^{4/11}$ $q''_{CHF,h} = 0.06h_{fg}\rho_g^{3/5}\sigma^{2/5}[g(\rho_f-\rho_g)/\mu_f]^{1/5}$ *for* $P/P_{crit} > 0.03$ $q''_{CHF} = (q''^3_{CHF,h} + q''^3_{CHF,I})^{1/3}$ *for* $0.001 < P/P_{crit} < 0.03$
Wang *et al.* [29]	$q''_{CHF} = [0.18 - 0.14(P/P_c)^{5.68}] \times \rho_g h_{fg}[\sigma g(\rho_f-\rho_g)/\rho_g^2]^{1/4}$
Case 2: saturated, 1g, infinite, all orientations.	
Chang [106]	$q''_{CHF} = C_{CHF}(\theta) \times 0.13\rho_g h_{fg}[\sigma g(\rho_f-\rho_g)/\rho_g^2]^{1/4}$ where $C_{CHF}(\theta) = \begin{cases} 1 & \theta = 0^\circ \\ 0.75 & \theta = 90^\circ \end{cases}$
Vishnev [116]	$q''_{CHF} = 0.0125(190-\theta)^{1/2}\rho_g h_{fg}[\sigma g(\rho_f-\rho_g)/\rho_g^2]^{1/4}$
El-Genk and Guo [117]	$q''_{CHF}(\theta) = C_{CHF}(\theta) \times \rho_g h_{fg}[\sigma g(\rho_f-\rho_g)/\rho_g^2]^{1/4}$ where $C_{CHF}(\theta) = \begin{cases} 0.034+0.0037(180-\theta)^{0.656} & \text{for water} \\ 0.033+0.0096(180-\theta)^{0.479} & \text{for nitrogen} \\ 0.002+0.0051(180-\theta)^{0.633} & \text{for helium} \end{cases}$
Chang and You [118]	$q''_{CHF}/q''_{CHF,max} = 1 - 0.0012\theta\tan(0.414\theta) - 0.122\sin(0.318\theta)$
Arik and Bar-Cohen [119]	$q''_{CHF} = 0.131(1 - 0.001117\theta + 7.79401 \times 10^{-6}\theta^2 - 1.37678 \times 10^{-7}\theta^3) \times \rho_g h_{fg}[\sigma g(\rho_f-\rho_g)/\rho_g^2]^{1/4}$
El Genk and Bostanci [120]	$q''_{CHF} = [(0.229 - 4.27 \times 10^{-4}\theta)^{-6} + (0.577 - 2.98 \times 10^{-3}\theta)^{-6}]^{-1/6} \times \rho_g h_{fg}[\sigma g(\rho_f-\rho_g)/\rho_g^2]^{1/4}$
Priarone [121]	$q''_{CHF,FC-72} = C_{CHF}(\theta) \times 0.165\rho_g h_{fg}[\sigma g(\rho_f-\rho_g)/\rho_g^2]^{1/4}$ $q''_{CHF,HFE-7100} = C_{CHF}(\theta) \times 0.21\rho_g h_{fg}[\sigma g(\rho_f-\rho_g)/\rho_g^2]^{1/4}$ where $C_{CHF}(\theta) = 1 - 0.001117\theta + 7.79401 \times 10^{-6}\theta^2 - 1.37678 \times 10^{-7}\theta^3$
Case 3: saturated, subcooled, 1g, infinite, horizontal.	
Kutateladze [122]	$q''_{CHF,sub} = 0.16\rho_g h_{fg}[\sigma g(\rho_f-\rho_g)/\rho_g^2]^{1/4} \times [1 + 0.065(\rho_f/\rho_g)^{0.8}(c_{p,f}\Delta T_{sub}/h_{fg})]$
Bonilla [123]	$q''_{CHF,sub} = q''_{CHF,sat} \times F_{sub}$ $F_{sub} = 1 + \left(\frac{\rho_f}{\rho_g}\right)^{0.923}\left(\frac{c_{p,f}\Delta T_{sub}}{25h_{fg}}\right)$
Zuber *et al.* [22]	$q''_{CHF} = \frac{\pi}{24}\rho_g h_{fg}\left[\sigma g\left(\frac{\rho_f-\rho_g}{\rho_g^2}\right)\right]^{1/4} + \frac{2k_f\Delta T_{sub}}{\sqrt{\pi\alpha_f\tau}}$ where $\tau = \frac{\pi}{3}\sqrt{2\pi}\left[\frac{\sigma}{g(\rho_f-\rho_g)}\right]^{1/2}\left[\frac{\rho_g^2}{\sigma g(\rho_f-\rho_g)}\right]^{1/4}$ and $\alpha_f = \frac{k_f}{\rho_f c_{p,f}}$

(*continued on next page*)

Table 5 (*continued*)

Author(s)	Model(s) or Correlation(s)
Ivey and Morris [124]	$q''_{CHF,sub} = q''_{CHF,sat} \times F_{sub}$ $F_{sub} = 1 + \left(\frac{\rho_f}{\rho_g}\right)^{0.75}\left(\frac{c_{p,f}\Delta T_{sub}}{9.8h_{fg}}\right)$
Wang *et al.* [29]	$q''_{CHF,sub} = K \times \rho_g\, h_{fg}[\sigma g(\rho_f - \rho_g)/\rho_g^2]^{1/4} \times [1 + 0.23(\rho_g/\rho_f)^{0.8}(c_{p,f}\Delta T_{sub}/h_{fg})]$
***Case 4:* saturated, subcooled, 1g, infinite, all orientations.**	
Hata *et al.* [29,72,80,125]	$q''_{CHF,sub} = 0.17\rho_g h_{fg}\left(\frac{\rho_f}{\rho_f+\rho_g}\right)^{1.5}\frac{1}{1+0.01\exp\{(2-0.33S_c)\theta\}} \times [\sigma g(\rho_f-\rho_g)/\rho_g^2]^{1/4}[1+0.065(\rho_f/\rho_g)^{0.8}S_c]$ where $S_c = (c_{p,f}\Delta T_{sub}/h_{fg})$ $\begin{cases} 0.16 \text{ recommended by Brentari et al.(1965)[125]} & \text{and Bewilogua et al.(1975)[80]} \\ [0.18 - 0.14(P/P_{crit})^{5.68}] & \text{recommended by Wang et al.(2016)[29]} \end{cases}$
El-Genk and Bostanci [126]	$q''_{CHF,sub} = C_{CHF}(\theta, \Delta T_{sub}) \times \rho_g h_{fg}[\sigma g(\rho_f-\rho_g)/\rho_g^2]^{1/4}$ $C_{CHF}(\theta, \Delta T_{sub}) = C_{CHF,\,sat}(\theta) \times R(\theta, \Delta T_{sub})$ $C_{CHF,sat}(\theta) = [(0.229 - 4.27 \times 10^{-4}\theta)^{-6} + (0.577 - 2.98 \times 10^{-3}\theta)^{-6}]^{-1/6}$ $R(\theta, \Delta T_{sub}) = [1 + (0.016 + 1.05 \times 10^{-4}\theta + 3.986 \times 10^{-7}\theta^2)\Delta T_{sub}]$
Brusstar and Merte [127,128]	$q''_{CHF} = \frac{\pi}{24}C_{CHF}(\theta) \times F_{sub} \times \rho_g\, h_{fg}[\sigma g(\rho_f-\rho_g)/\rho_g^2]^{1/4}$ where $C_{CHF}(\theta) = \begin{cases} 1.0 & 0^\circ \le \theta < 90^\circ \\ \lvert\sin\theta\rvert^{1/2} & 90^\circ \le \theta \le 180^\circ \end{cases}$ and $F_{sub} = 1 + \left(\frac{\rho_f}{\rho_g}\right)^{0.75}\left(\frac{c_{p,f}\Delta T_{sub}}{9.8h_{fg}}\right)$
***Case 5:* saturated, 1g, infinite, horizontal, contact angle.**	
Chang and Snyder [105]	$q''_{CHF} = \frac{1}{2}\left(\frac{\pi}{6}\right)^{5/6}(0.0119\alpha)^{1/2}\rho_g h_{fg}[2\sigma g(\rho_f-\rho_g)/\rho_g^2]^{1/4}$
Kirichenko and Chernyakov [129]	$q''_{CHF} = 0.171\frac{(1+0.324\times10^{-3}\alpha^2)^{1/4}}{(0.018\alpha)^{1/2}}\rho_g h_{fg}[\sigma g(\rho_f-\rho_g)/\rho_g^2]^{1/4}$
Theofanous and Dinh [16]	$q''_{CHF} = k^{-1/2}\rho_g h_{fg}[\sigma g(\rho_f-\rho_g)/\rho_g^2]^{1/4}$ where $k = \left(1 - \frac{\sin\alpha}{2} - \frac{\pi/2-\alpha}{2\cos\alpha}\right)^{-1/2}$ derived by Kim *et al.* [130]
***Case 6:* saturated, 1g, infinite, all orientations, contact angle.**	
Kandlikar [131]	$q''_{CHF} = \frac{1+\cos\alpha}{16}\left[\frac{2}{\pi} + \frac{\pi}{4}(1+\cos\alpha)\cos\theta\right]^{1/2} \times \rho_g h_{fg}[\sigma g(\rho_f-\rho_g)/\rho_g^2]^{1/4}$
Liao *et al.* [132]	$q''_{CHF} = 0.131\left[-0.73 + \frac{1.73}{1+10^{-0.021\times(185.4-\theta)}}\right]\left[1 + \frac{55-\alpha}{100}(0.56 - 0.0013\theta)\right] \times \rho_g h_{fg}[\sigma g(\rho_f-\rho_g)/\rho_g^2]^{1/4}$
***Case 7:* saturated, 1g, infinite, horizontal, conduction.**	
Golobič and Bergles [133]	$\frac{q''_{CHF}}{q''_{CHF,asy}} = 1 - \exp\left[-\left(\frac{S}{2.44}\right)^{0.8498} - \left(\frac{S}{2.44}\right)^{0.0581}\right]$ where $S = H\sqrt{(\rho c_p k)_w}$
***Case 8:* saturated, subcooled, 1g, infinite, horizontal, conduction.**	
Watwe and Bar-Cohen [134]	$q''_{CHF,sub} = \frac{\pi}{24}\left(\frac{S}{S+0.1}\right)\left\{1 + \left(0.3014 - 0.01507L\sqrt{\frac{g(\rho_f-\rho_g)}{\sigma}}\right)\right\} \times \left\{1 + 0.03\left[\left(\frac{\rho_f}{\rho_g}\right)^{3/4}\frac{c_{p,f}}{h_{fg}}\right]\Delta T_{sub}\right\} \times$ $\rho_g h_{fg}[\sigma g(\rho_f-\rho_g)/\rho_g^2]^{1/4}$ where $S = H\sqrt{(\rho c_p k)_w}$
Case 9: saturated, 1g, infinite, horizontal, contact angle, roughness.	
Ramilison *et al.* [135]	$q''_{CHF} = 0.0044(\pi-\alpha)^3 R_a^{0.125} \times \rho_g\, h_{fg}[\sigma g(\rho_f-\rho_g)/\rho_g^2]^{1/4}$
Kim *et al.* (2016) [136]	$q''_{CHF} = 0.811\left(\frac{1+\cos\alpha}{16}\right)\left[\frac{2}{\pi} + \frac{\pi}{4}(1+\cos\alpha) + \frac{351.2\cos\alpha}{1+\cos\alpha}\left(\frac{R_a}{S_m}\right)\right]^{1/2} \times \rho_g h_{fg}[\sigma g(\rho_f-\rho_g)/\rho_g^2]^{1/4}$
Case 10: saturated, 1g, finite, horizontal.	
Lienhard and Dhir [108,109]	$q''_{CHF} = \left(\frac{\pi}{A_h}\frac{\sigma}{g(\rho_f-\rho_g)}\right)^{1/4}\left(\frac{A_j}{A_h}\right)^{3/4} \times \rho_g h_{fg}[\sigma g(\rho_f-\rho_g)/\rho_g^2]^{1/4}$ where $\frac{A_j}{A_h} \simeq 0.155$Note: valid for all configuration except for the case of small spheres and infinite flat plate

μ_f: liquid viscosity, α: contact angle, P: pressure, P_c: critical pressure, R_a: surface roughness, S: thermal activity parameter, $c_{p,f}$: specific heat of liquid at constant pressure, ΔT_{sub}: liquid subcooling, S_m: mean spacing between surface roughness peaks.

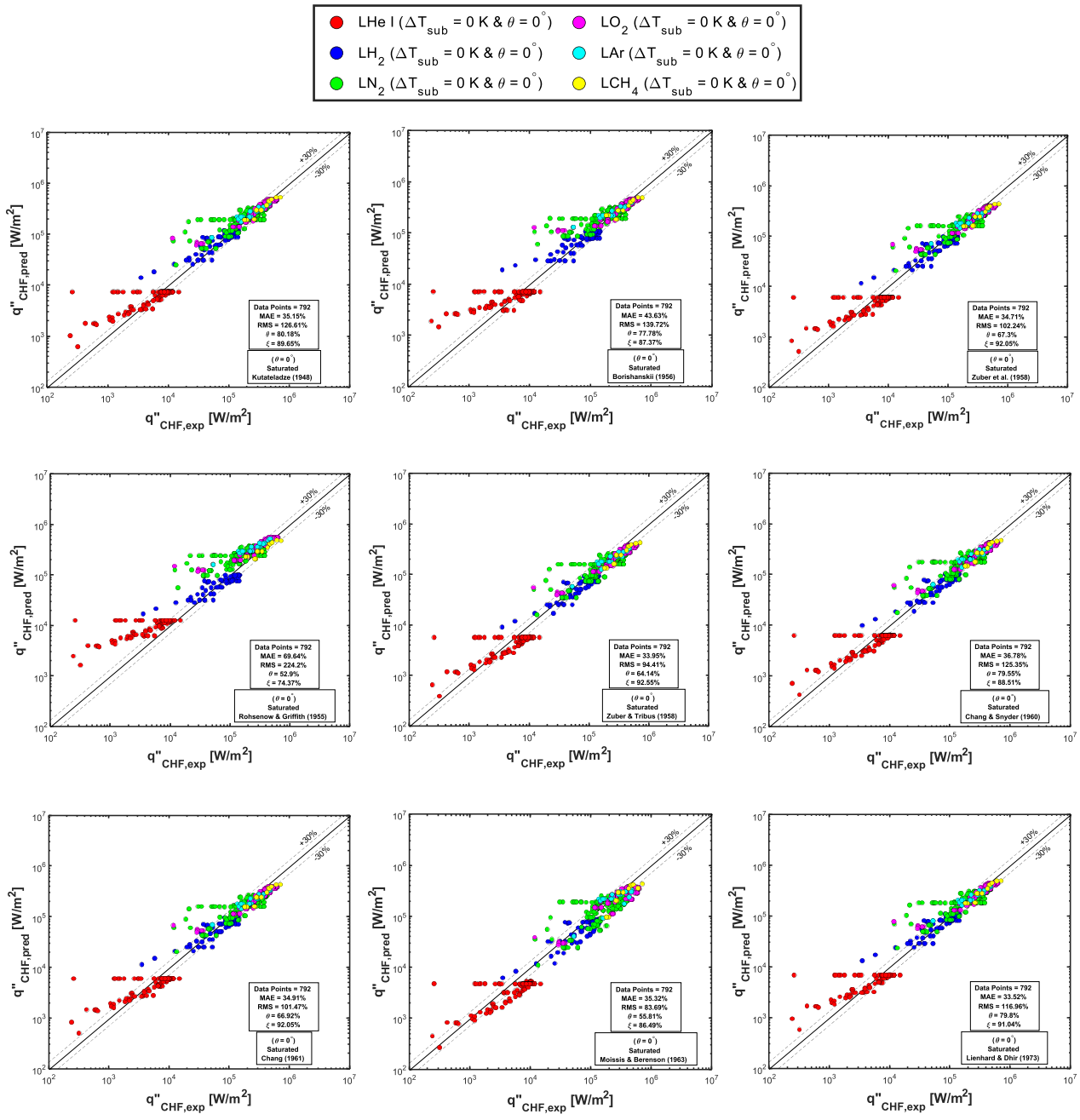

Fig. 5. Assessment of CHF models and correlations for saturated 1-g pool boiling from infinite horizontal surfaces (Case 1).

thickness [113]), Sakashita and Ono [111] (using Rajvanshi's macrolayer thickness [112]), and Guan et al [115]., are associated with comparatively high MAEs of 69.64%, 89.27%, 63.93%, and 51.99%, respectively.

Notice how certain data points appear to depart significantly from predictions of most models and correlations in Figs. 5 and 6. Data outliers are demarcated in Fig. 7 by the trapezoidal area in the comparison of Zuber et al.'s [14,22] predictions versus experimental data. These high MAE outliers were found to consist of CHF data (i) near critical pressure, (ii) measured using stainless steel heating surface, (iii) corresponding to very high surface roughness, or (iv) or departing significantly from data of majority of studies (*e.g.,* data from Grigor'ev et al [86]. and Ishigai et al [91].). Identifying data outliers is crucial to developing a new model or correlation. This important issue will be discussed in a later section.

4.2.2. Correlations considering orientation effects (Case 2)

A total of 1111 data points are used to assess 6 different correlations that incorporate the effect of orientation. It is noted that El-Genk and Guo [117] recommended adjusting their correlation using different multipliers for three different fluids (water, nitrogen and helium) and recommended a different multiplier for each fluid. Similarly, Priarone [121] recommended different multipliers for FC-72 and HFE-7100. Hence, these correlations are assessed separately with each multiplier value using the entire 1111 data points. One exception is the correlation by Chang and You [118] which requires using measured CHF value for a horizontal upward facing orientation to predict CHF for inclined surfaces. This reduced the database used to assess this particular correlation to only three fluids (LHe, LH_2 and LN_2) and 203 datapoints.

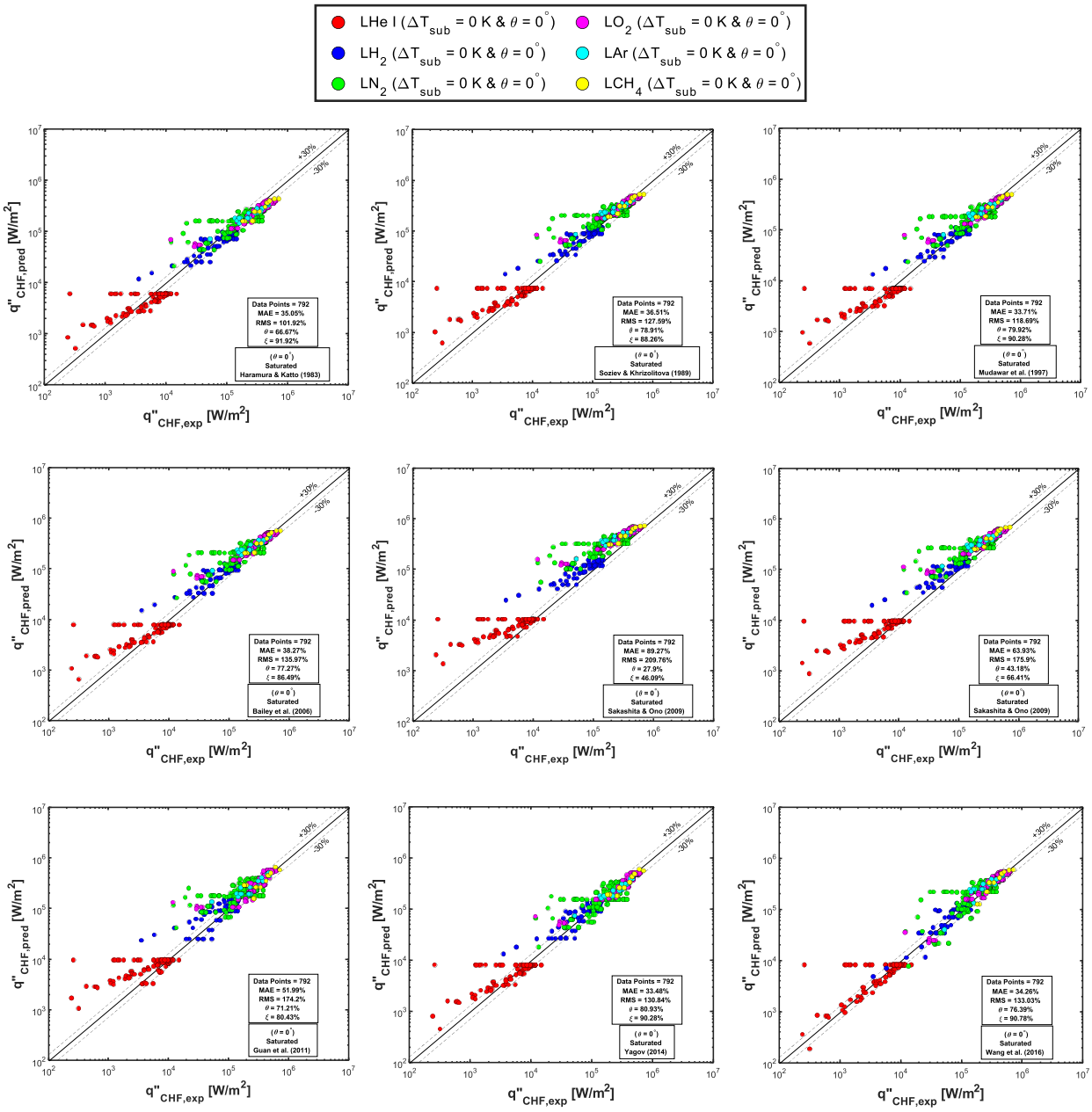

Fig. 6. Assessment of CHF models and correlations for saturated 1-g pool boiling from infinite horizontal surfaces (case 1) (continued).

A summary of the assessment study for Case 2 is provided in Table 6, with a comparison of predicted versus measured CHF for each correlation shown in Fig. 8. Overall, best predictions are achieved using the correlation of El-Genk and Guo [117], with MAEs of 34.84%, 34.9% and 35.43% using multipliers for water, nitrogen and helium, respectively, followed by Vishnev [116], 39.68%, Arik and Bar-Cohen [119], 35.53%, and Priarone [121] (using FC-72 multiplier), 39.44%. Lesser accuracy is achieved with the correlations by Chang [106], 50.59%, Priarone [121] (using HFE-7100 multiplier), 65.21%, and El-Genk and Bostanci [120], 74.7%. For the special correlation by Chang and You [118], MAE is 29.48%, albeit for only a subset of the Case 2 database.

4.2.3. Correlations considering subcooling effects (Case 3)

Five different Case 3 correlations are assessed using a database consisting of all six fluids and 873 data points. A summary of assessment results is provided in Table 6, with a comparison of predicted versus measured CHF for each correlation shown in Fig. 9. Overall, best predictions are achieved with the correlation by Wang et al [29]., evidenced by its lowest MAE of 33.42%. It is followed closely by the correlations of Bonilla [123], 34.03%, Kutateladze [122], 34.03%, and Ivey and Morris [124], 34.29%. On the other hand, the correlation by Zuber *et al.* [22] shows a rather high MAE of 54.97%, indicating overestimation of subcooling effects.

4.2.4. Correlations considering combined effects of orientation and subcooling (Case 4)

Three different correlations capable of addressing the combined effects of orientation and subcooling are assessed against a total of 1239 data points for all fluids, with results provided in Table 6 and Fig. 10. The correlation by Hata *et al.* [72] is shown yielding the best accuracy, with a MAE of 30.39%, followed closely by Brustar and Merte [127,128], 35.26%. On the other hand, the correlation by El-Genk and Bostanci [126] yields a relatively high MAE of 71.89%.

Table 6
Summary of assessment study.

	MAE %	RMS %	% of points within ±30%	% of points within ±50%	Number of data points
Case 1					
Kutateladze [20]	35.15	126.61	80.18	89.65	792
Rohsenow and Griffith [13]	69.64	224.2	52.9	74.37	792
Borishanskii [103]	43.63	139.72	77.78	87.37	792
Zuber *et al.* [14,22]	34.71	102.24	67.3	92.05	792
Zuber and Tribus [104]	33.95	94.41	64.14	92.55	792
Chang and Snyder [105]	36.78	125.35	79.55	88.51	792
Chang [106]	34.91	101.47	66.92	92.05	792
Moissis and Berenson [107]	35.32	83.69	55.81	86.49	792
Lienhard and Dhir [108,109]	33.52	116.96	79.8	91.04	792
Haramura and Katto [15]	35.05	101.92	66.67	91.92	792
Soziev and Khrizolitova [110]	36.51	127.59	78.91	88.26	792
Sakashita and Ono [111,113]	89.27	209.76	27.9	46.09	792
Sakashita and Ono [111,112]	63.93	175.9	43.18	66.41	792
Mudawar *et al.* [18]	33.71	118.69	79.92	90.28	792
Bailey *et al.* [114]	38.27	135.97	77.27	86.49	792
Gaun *et al.* [115]	51.99	174.2	71.21	80.43	792
Yagov [17]	33.48	130.84	80.93	90.28	792
Wang *et al.* [29]	34.26	133.03	76.39	90.78	792
Case 2					
Chang [106]	50.59	195.04	61.48	87.13	1111
Vishnev [116]	39.68	134.57	75.61	85.69	1111
El-Genk and Guo (for water) [117]	34.84	111.92	76.06	90.37	1111
El-Genk and Guo (for nitrogen) [117]	34.9	113.17	76.69	89.47	1111
El-Genk and Guo (for helium) [117]	35.43	94.71	64.45	87.58	1111
Chang and You [118]	29.48	42.04	62.07	80.79	203
Arik and Bar-Cohen [119]	35.53	102.24	67.78	90.55	1111
El Genk and Bostanci [120]	74.7	181.34	30.69	56.26	1111
Priarone (for FC-72) [121]	39.44	131.89	74.98	86.41	1111
Priarone (for HFE-7100) [121]	65.21	175.8	44.37	67.51	1111
Case 3					
Kutateladze [122]	34.08	120.88	77.78	90.61	873
Bonilla [123]	34.03	120.87	78.24	90.61	873
Zuber *et al.* [22]	54.97	161.4	63.57	86.71	873
Ivey and Morris [124]	34.29	120.92	77.66	90.26	873
Wang *et al.* [29]	33.42	126.99	74.8	91.64	873
Case 4					
Hata *et al.* [72]	30.39	92.41	70.86	91.44	1239
El-Genk and Bostanci [126]	71.89	172.69	31.4	55.93	1239
Brusstar and Merte [127,128]	35.26	87.28	64.89	87.17	1239
Case 5					
Chang and Snyder [105]	49.53	128.17	42.05	65.66	792
Kirichenko and Chernyakov [129]	285.73	431.01	1.77	6.57	792
Theofanous and Dinh [16,130]	406.06	653.24	0	0	792
Case 6					
Kandlikar [131]	40.68	131.47	68.23	85.13	982
Liao *et al.* [132]	40.49	124.91	71.92	83.98	1111
Case 7					
Golobič and Bergles [133]	42.53	65.27	34.65	85.15	202
Case 8					
Watwe and Bar-Cohen [134]	64.99	96.45	36.8	52	250
Case 9					
Ramilison *et al.* [135]	49.45	102.04	54.26	80.62	129
Case 10					
Lienhard and Dhir [108,109]	46.59	73.76	29.92	60.1	782

4.3. Correlations assessed using portions of consolidated database missing values for essential surface parameters

4.3.1. Correlations considering contact angle effects (Case 5)

It must be noted that published contact angle information is quite sparse. In the present assessment study, contact angle information for LO_2 and LN_2 is obtained from a NASA Technical Report by Brennan and Skrabek [137], LH_2 from Bellur *et al.* [138] and Konduru [139] and, due to lack of information, contact angles for LHe1, LAr and LCH_4 are assumed constant, 20°, as per Kandlikar [131].

Detailed correlation assessment results for Case 5 are provided in Table 6 and Fig. 11. With a MAE of 49.53%, the correlation by Chang and Snyder [105] provides the most superior accuracy, while those by Kirichenko and Chernyakov [129] and Theofanous and Dinh [16,130] show poor predictions, 285.73% and 406.06%, respectively.

Overall, lack of detailed contact angle information for most cryogens and variations of contact angle with surface finish or coating (which are absent from most literature) preclude incorporating this effect in the proposed new universal CHF correlation for cryogens. However, the universal correlation may be modified

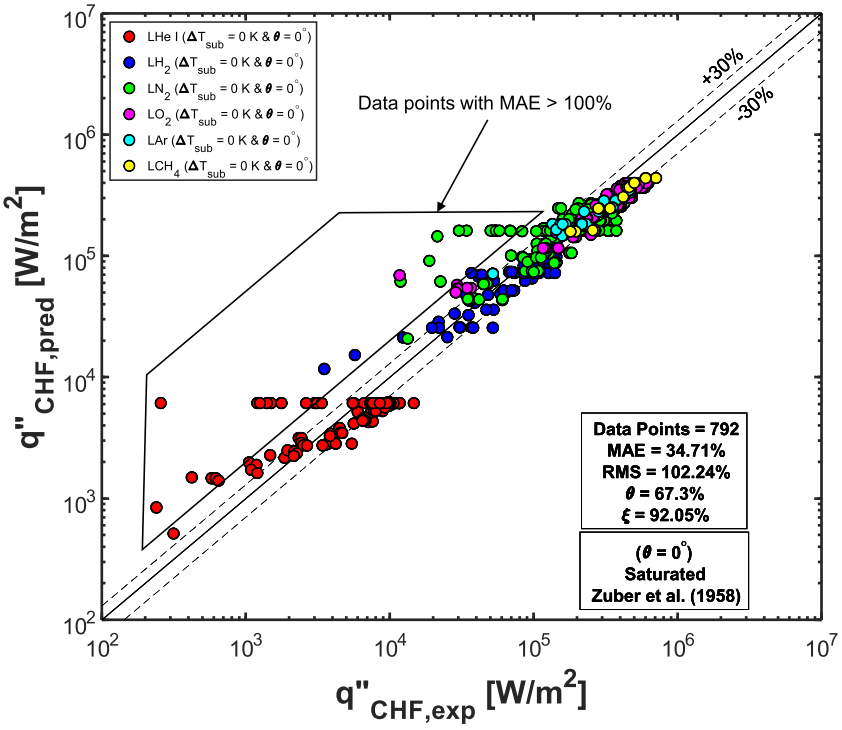

Fig. 7. Identification of data outliers.

in the future after systematic measurements are made for all six cryogens and different surface types.

4.3.2. Correlations considering combined orientation and contact angle effects (Case 6)

Detailed assessment results for Case 6 are provided in Table 6 and Fig. 12. Here, different data subsets are used when assessing the correlation by Kandlikar [131] (which is restricted to angles between 0 and 90°), 982 points, versus Liao *et al.* [132] (which is valid for angles between 0 and 180°), 1111 points. The two correlations yield fairly similar values for MAE, 40.68% versus 40.49%, respectively.

Here too, absent reliable contact angle data for Case 6, incorporating this effect in the proposed new universal CHF correlation for cryogens is unwarranted.

4.3.3. Correlations considering conduction effects (Case 7)

For Case 7, assessment of a correlation by Golobič and Bergles [133] required relying on a much smaller database after excluding data for which either heating surface thickness or properties are unavailable from original data references. Results from Table 6 and Fig. 13 show this correlation has a MAE of 42.53% corresponding to a subset of 202 datapoints for horizontal upward-facing orientation.

Given the limited subset of the Consolidated Database for which both wall material and thickness information is provided, this effect is avoided when developing the new universal correlation.

4.3.4. Correlations considering combined conduction and subcooling effects (Case 8)

Similar to Case 7, assessment of a correlation by Watwe and Bar-Cohen [134] relied on a rather small subset of 250 CHF datapoints. The assessment results are provided in Table 6 and Fig. 14, which reveal a rather high MAE of 64.99% evidenced by inaccurate predictions for all fluids except LO_2.

Here too, with only a small subset of the Consolidated Database including both wall material and thickness information is provided, this effect is avoided when developing the new universal correlation.

4.3.5. Correlations considering combined surface roughness and contact angle effects (Case 9)

Overall, information regarding surface material and thickness are available in majority of references, and most involve use of smooth, polished or rolled surfaces for which roughness information is generally lacking. This reduced the number of datapoints available for assessment of Case 9 to only 129. Here, a single correlation by Ramilison *et al.* [135] yielded a MAE of 49.45%, as indicated in Table 6 and Fig. 15.

Given the limited subset of the Consolidated Database for which wall material, wall thickness, and surface roughness information is provided, this effect is avoided when developing the new universal correlation.

4.3.6. Correlations considering finite heater size effects (Case 10)

CHF correlations and models developed for an infinite heated surface should yield good predictions for a finite surface with characteristic length much larger than the Taylor most dangerous wavelength, λ_d. This ensures that the hydrodynamic instability responsible for initiating vapor jets perpendicular to the heating surface remains intact. On the other hand, a surface with a characteristic length approaching or smaller than λ_d would alter altogether the formation of the vapor jets and therefore size will have a strong influence on CHF. Lienhard and Dhir [108,109] suggested that CHF for a surface with ratio of characteristic length to λ_d of 3 or greater will be close to that of an infinite surface, while a surface with a ratio below 3 must be treated as 'finite' because of the influence of size on CHF. They also developed a correlation for small finite surfaces [108,109]. A summary of the assessment results for this correlation using the smallest characteristic length is provided in Table 6 and Fig. 16, which indicate a MAE of 46.59%.

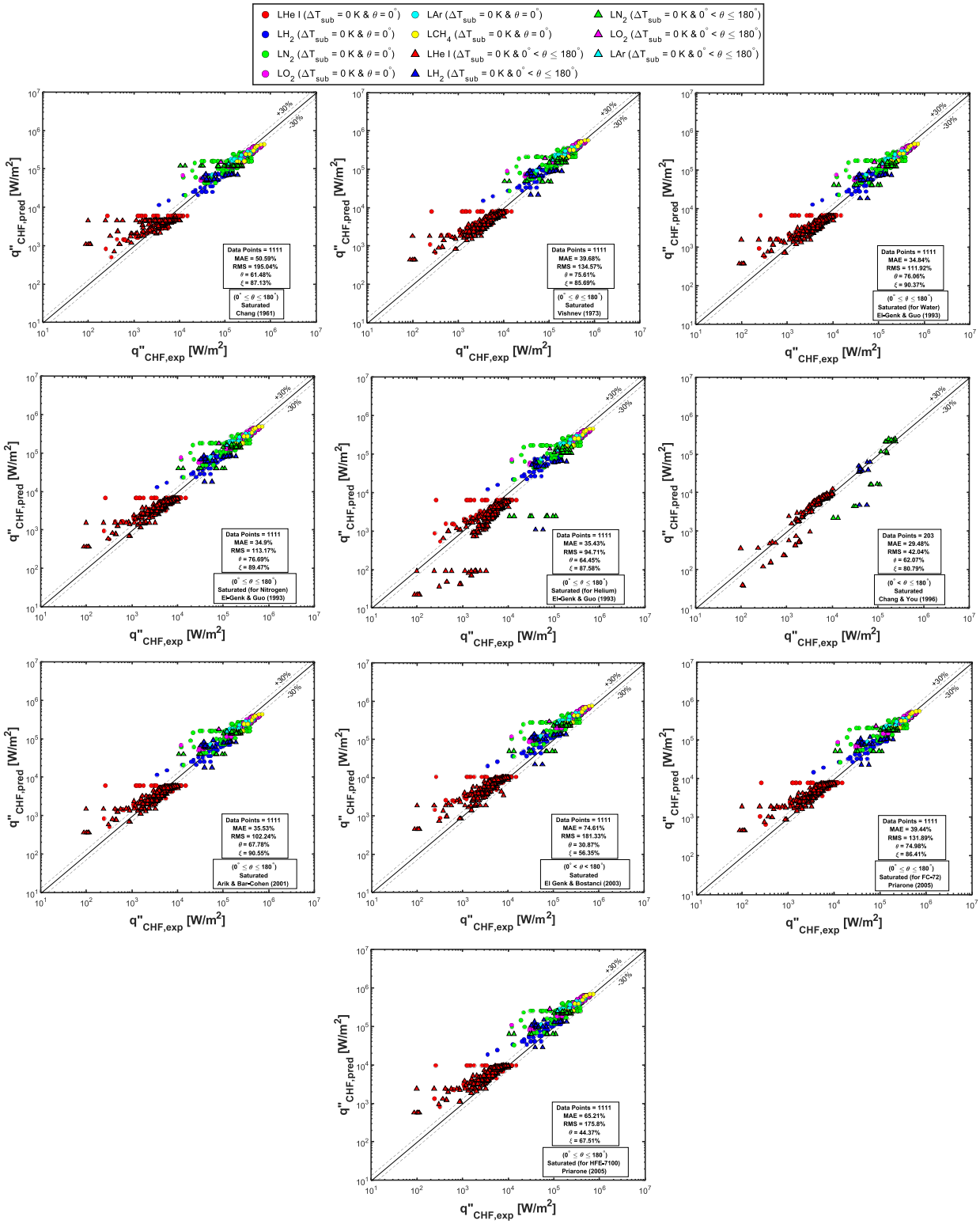

Fig. 8. Assessment of CHF models and correlations for saturated 1-g pool boiling from infinite surfaces at different orientations (Case 2).

It is important to note that, according to [108,109], surfaces with different shapes and rations of characteristic length to λ_d will require employing different dimensionless terms in the CHF correlation. Therefore, with an aim to develop a new universal CHF correlation in the present study, effects of finite surface size are avoided.

4.4. Summary of assessment results for all cases

Fig. 17 provides a summary of statistical results for all 10 cases, namely MAE, RMS, % of data within ±30% of predictions (θ), and % of data within ±50% of predictions (ξ). Notice how a good number of the models and correlations have MAE values below 40%, but

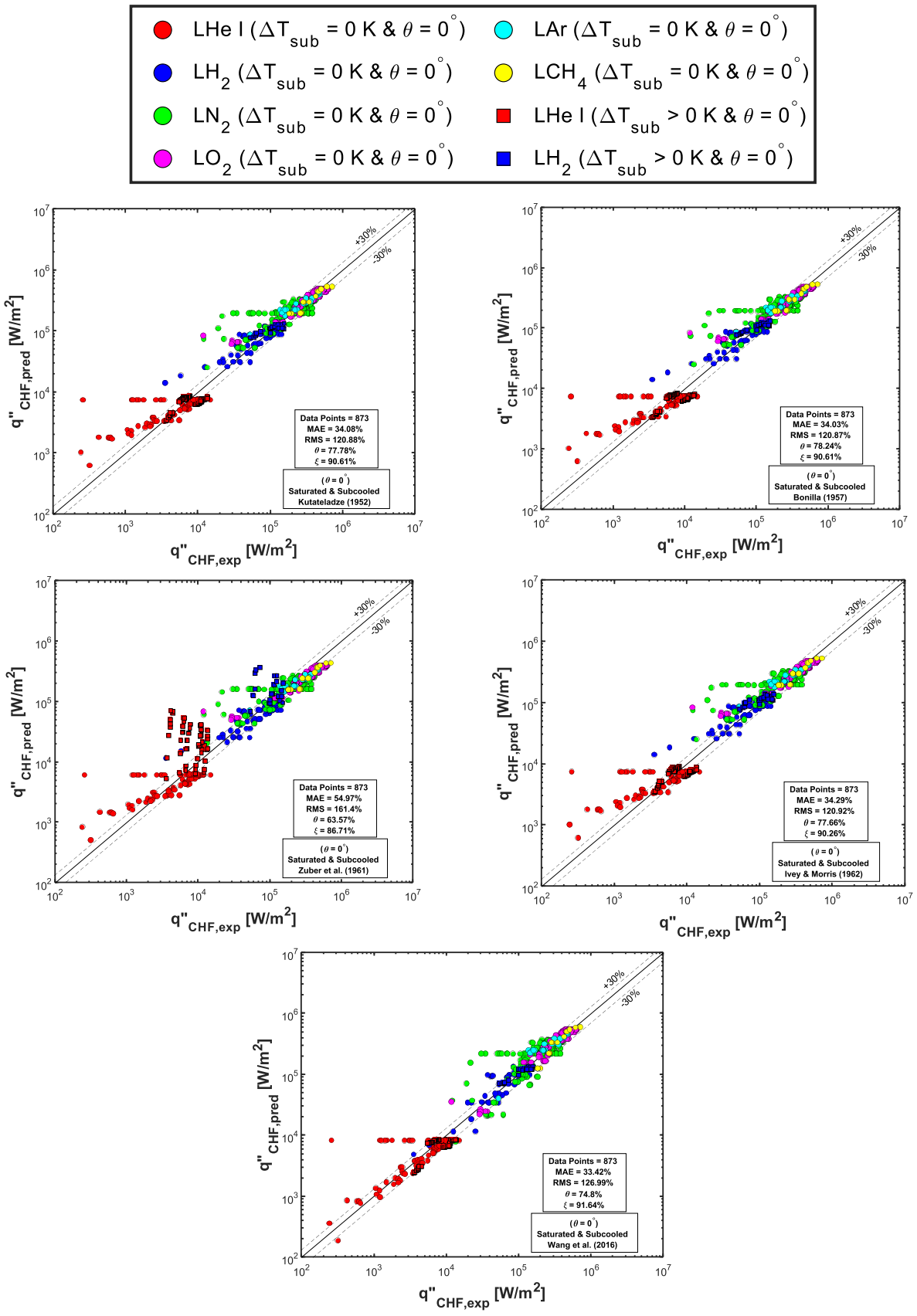

Fig. 9. Assessment of CHF models and correlations for saturated and subcooled 1-g pool boiling from infinite horizontal surfaces (Case 3).

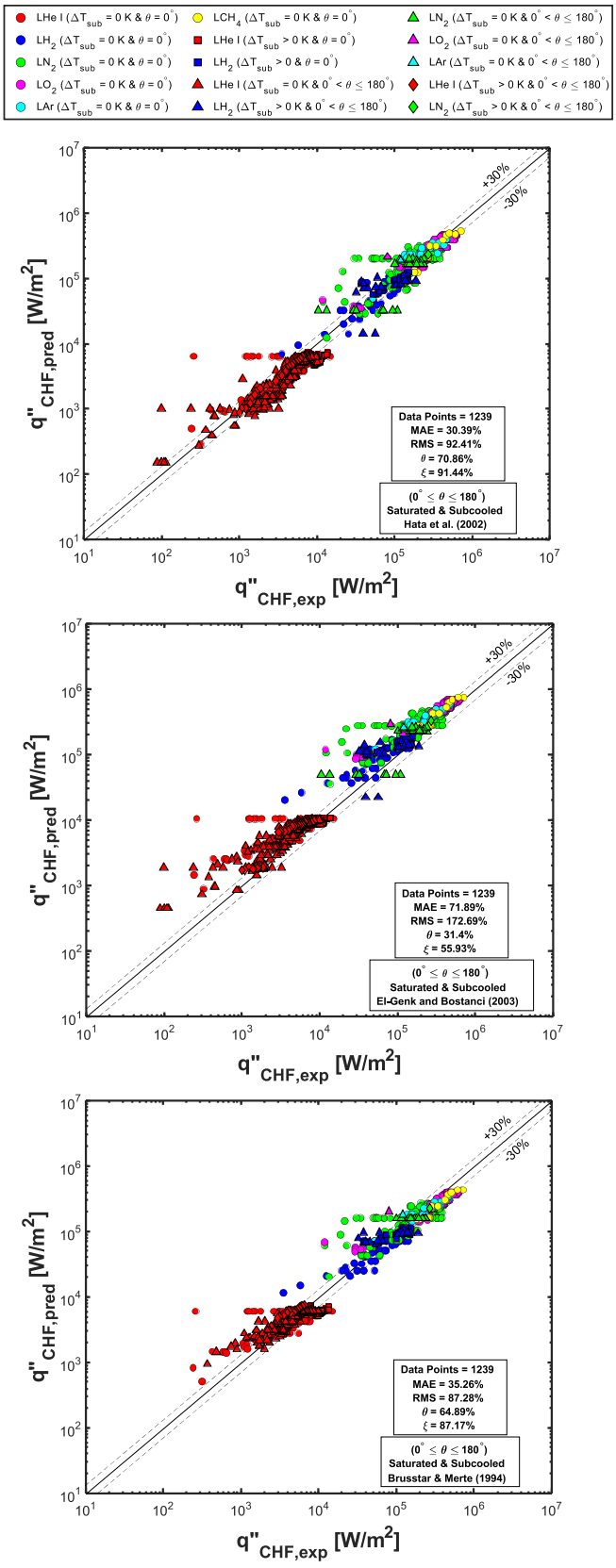

Fig. 10. Assessment of CHF correlations for saturated and subcooled 1-g pool boiling from infinite surfaces at different orientations (Case 4).

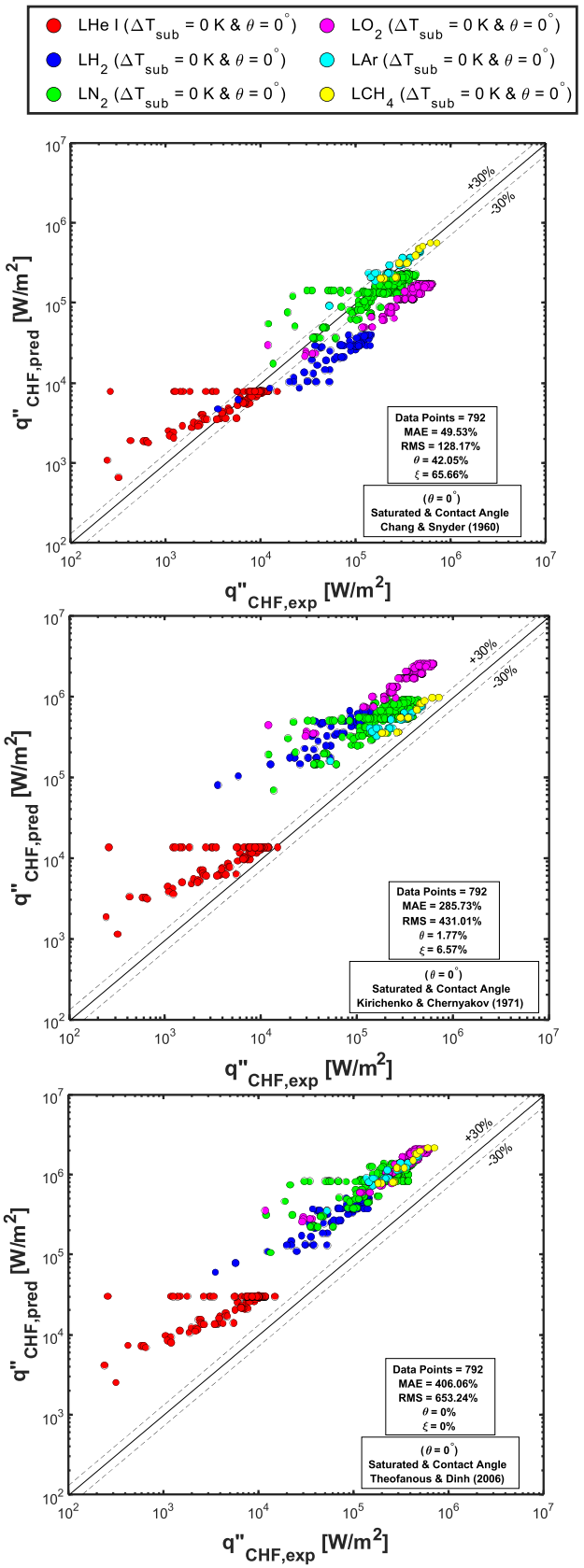

Fig. 11. Assessment of CHF correlations for saturated 1-g pool boiling from infinite horizontal surfaces, which also account for contact angle effects (Case 5).

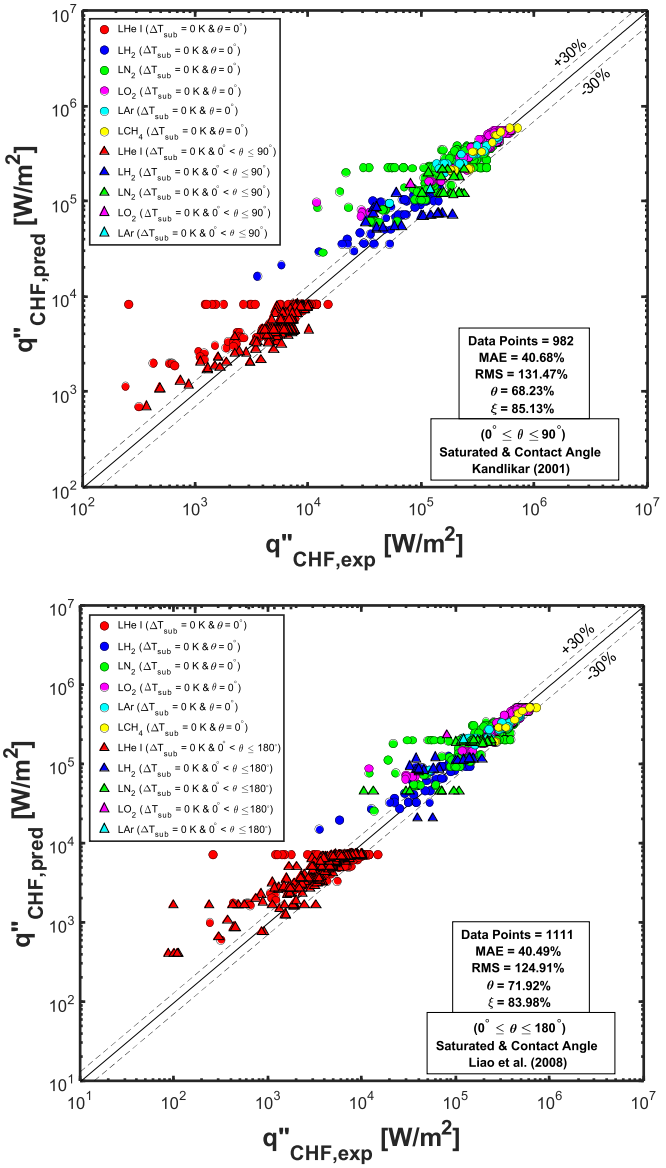

Fig. 12. Assessment of CHF correlations for saturated 1-g pool boiling from infinite surfaces at different orientations, which also account for contact angle effects (Case 6).

RMS is above 100% for most. Also shown is that percentages of data within ±30% and ±50% for a good number of the models and correlations are within 65-85% and 85-90%, respectively.

5. Assessment of predictive accuracy of correlations using reduced gravity data

Reduced gravity can have profound effects on pool boiling, especially CHF. Furthermore, assessment of reduced gravity effects is highly complicated by the influence of heater size. As indicated in Section 4.11, use of available models and correlations requires employing a heating surface with a ratio of characteristic length to λ_d of 3 or greater. Herein lies the difficulty in assessing predictive tools for reduced gravity Fig. 18. shows a plot of λ_d versus reduced gravity, a/g, for different fluids at atmospheric pressure. Notice how λ_d is quite small (centimeter range) for $a/g = 1$ but increases to the meter range for $a/g = 10^{-4}$ and tends to infinity for zero gravity. Clearly, heating surfaces used in low gravity pool boiling experiments are never sized to exceed $3\lambda_d$, especially those intended for microgravity.

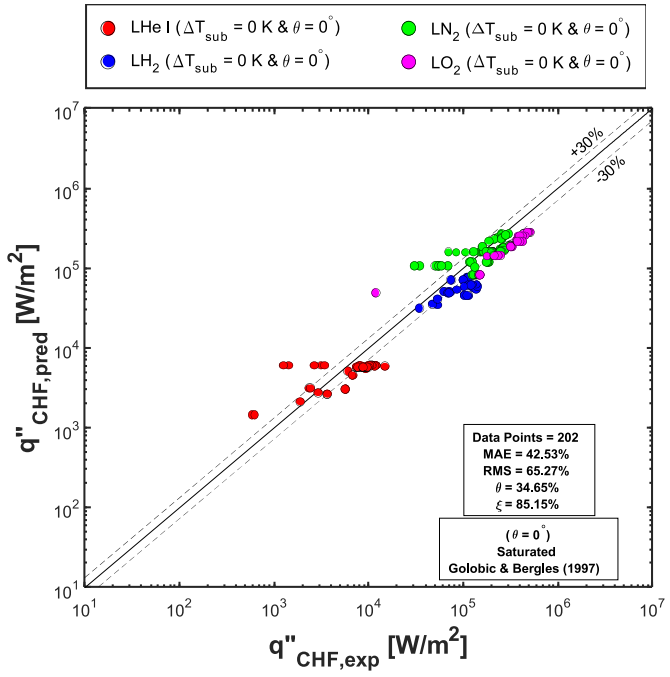

Fig. 13. Assessment of CHF correlation for saturated 1-g pool boiling from infinite horizontal surfaces, which also account for wall conduction effects (Case 7).

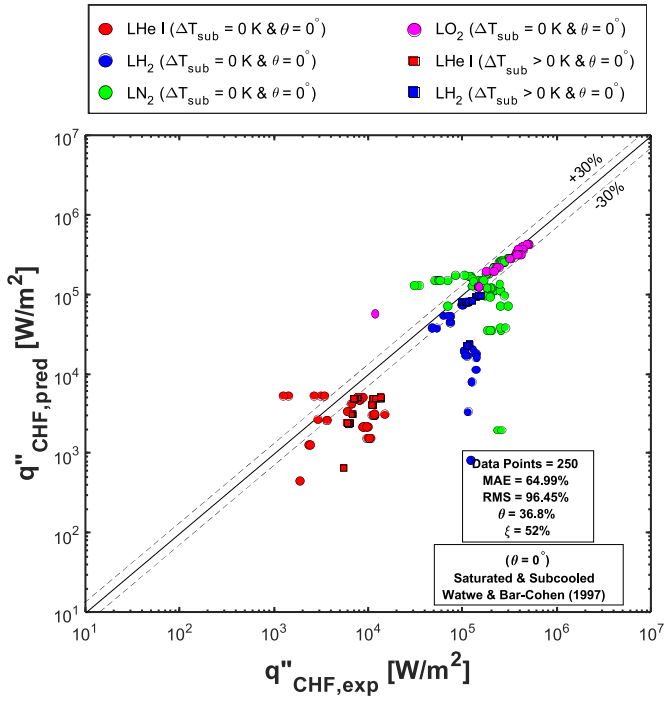

Fig. 14. Assessment of CHF correlation for saturated and subcooled 1-g pool boiling from infinite horizontal surfaces, which also account for wall conduction effects (Case 8).

Despite the shortcoming of reduced gravity studies in failing to meet the size requirement, 34 available reduced gravity CHF datapoints from three references, Garcia [28], Merte [47] and Lyon *et al.* [35], are compared to predictions of correlations by Chang and Snyder [105], Wang *et al.* [29], and El-Genk and Guo [117], each multiplied by the reduced gravity factor $(a/g)^{1/4}$. Results of the as-

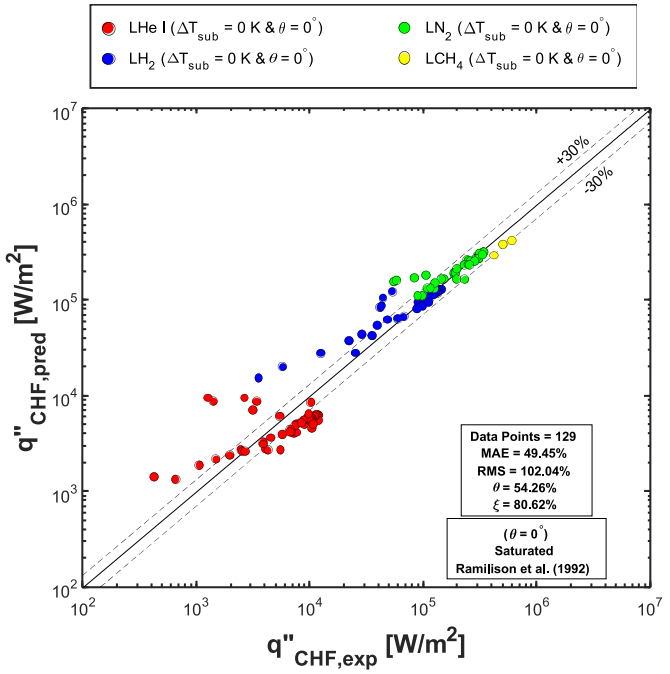

Fig. 15. Assessment of CHF correlation and models for saturated 1-g pool boiling from infinite horizontal surfaces, which also account for contact angle and surface roughness effects (Case 9).

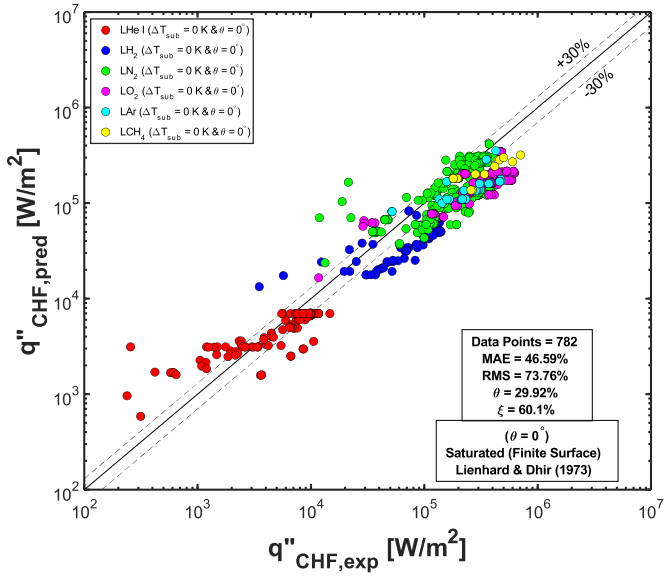

Fig. 16. Assessment of CHF correlation for saturated 1-g pool boiling from horizontal finite surfaces (Case10).

sessment are provided in Table 7, with Fig. 19 showing prediction plots. All three correlations are shown underpredicting the data, evidenced by MAEs of 60.23%, 56.99%, and 62.83%, respectively, a conclusion reminiscent of one made earlier by Lyon *et al.* [35].

6. New universal CHF correlations

6.1. Identification and additional exclusion of data outliers

The detailed assessment of CHF models and correlations presented thus far is based on a carefully compiled Consolidated Database arrived at after excluding duplicate and physically incompatible datapoints. However, as shown earlier in Fig. 7, the assessment study also revealed data outliers that requires further investigation and possible exclusion before attempting to develop a new improved CHF correlation. Most notably, they consist of a few datapoints which depart appreciably from the majority of published data for same fluids and similar operating conditions. Details of these outliers and reasons for their exclusion from the Consolidated Database are provided in Table 8.

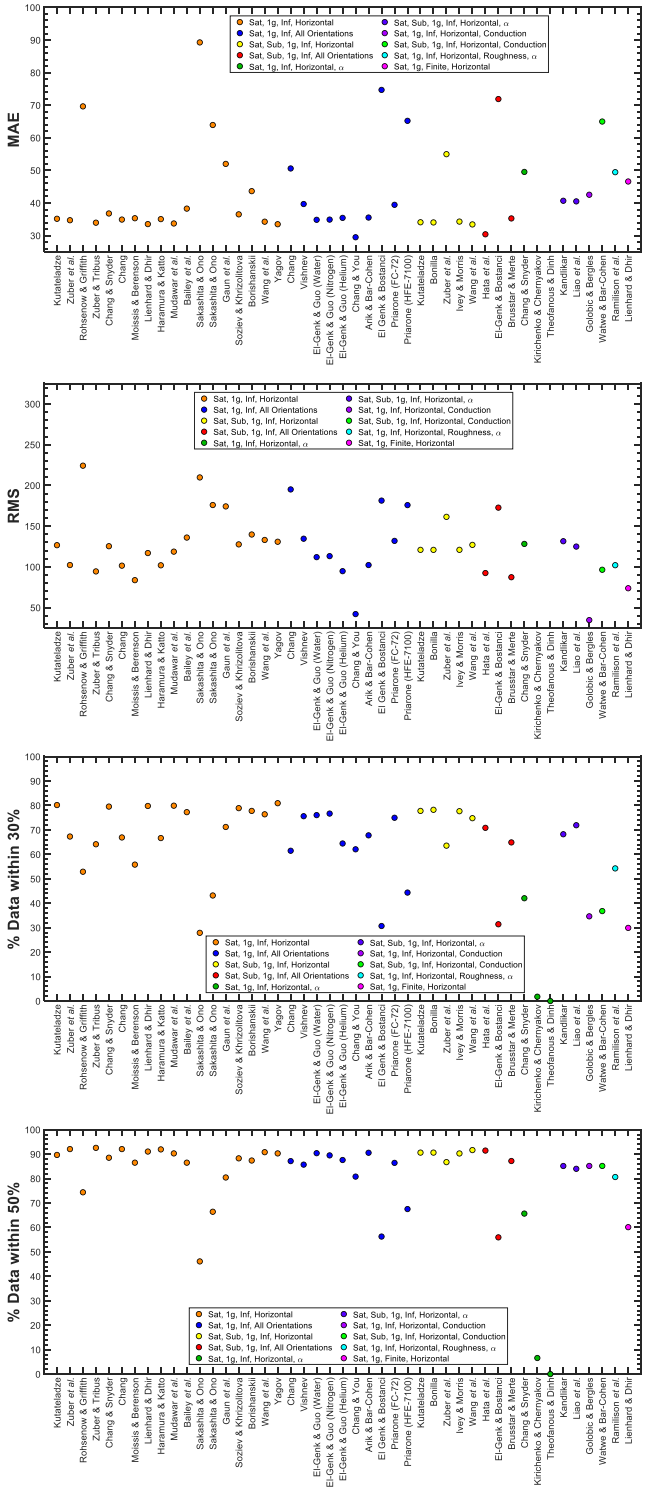

Fig. 17. Summary of statistical results of assessment study.

Table 7
Summary of assessment study using reduced gravity data.

	MAE %	RMS %	% of points within ±30%	% of points within ±50%	Number of data points
Chang and Snyder [105]	60.23	63.59	5.88	38.24	34
Wang *et al.* [29]	56.99	63.42	14.71	44.12	34
El-Genk and Guo (for water) [117]	62.83	66.29	5.88	32.35	34

Table 8
Additional exclusion of data outliers.

Refs.	No. of data points	Reason
Liquid Helium		
Lyon [36]	3	• Data obtained near critical pressure
Bewilogua *et al.* [80]	2	• Data obtained near critical pressure
Grigoriev *et al.* [54]	5	• Entire dataset from this reference associated with very high MAEs
Vishnev *et al.* [81]	2	• Data obtained for horizontal downward facing surface
Grigoriev *et al.* [86]	5	• Data obtained from heated surface with large surface roughness
Liquid Hydrogen		
Class *et al.* [32]	13	• Investigators mentioned that their CHF data are slightly lower than true CHF
Bewilogua *et al.* [80]	2	• Data obtained near critical pressure
Liquid Nitrogen		
Akhmedov *et al.* [89]	2	• Data obtained near critical operating
Ishigai *et al.* [91]	13	• Entire dataset from this reference associated with very high MAEs
Jin *et al.* [95]	1	• Data obtained from stainless steel surface with poor axial conductivity
Liquid Oxygen		
Lyon *et al.* [34]	1	• Data obtained near critical pressure
Lyon *et al.* [35]	4	• Normalized CHF values with test surface located 17.4 cm below midplane drop precipitately when the relative acceleration based upon bulk-liquid temperatures and the magnetic force at the surface fall below 0.025 • These data points are outliers because calculation of vapor acceleration is different compared to other data due to different test surface location in magnetic field
Total	***53***	

6.2. Parametric distribution of final cryogenic database

After exclusion of the data outliers, the final Consolidated Database contains 1218 data points corresponding to six fluids: LHe, LN_2, LH_2, LO_2, LAr, and LCH_4 Fig. 20. shows the number of CHF datapoints from experiments for different cryogenic fluids spanning six decades in the form of histograms versus (a) year of study, (b) system pressure, P, (c) reduced pressure, P_R, (d) subcooling, ΔT_{sub}, (e) heated surface orientation angle, θ, and (f) CHF magnitude.

While compiling the final Consolidated Database, it was observed that certain information important to comprehensive assessment of models and correlations is missing or sparse. This information consists mostly of gaps in the cryogenic pool boiling CHF data, identification of which might help in conducting systematic experiments in future studies. Recommendations to fill these data gaps can be summarized as follows:

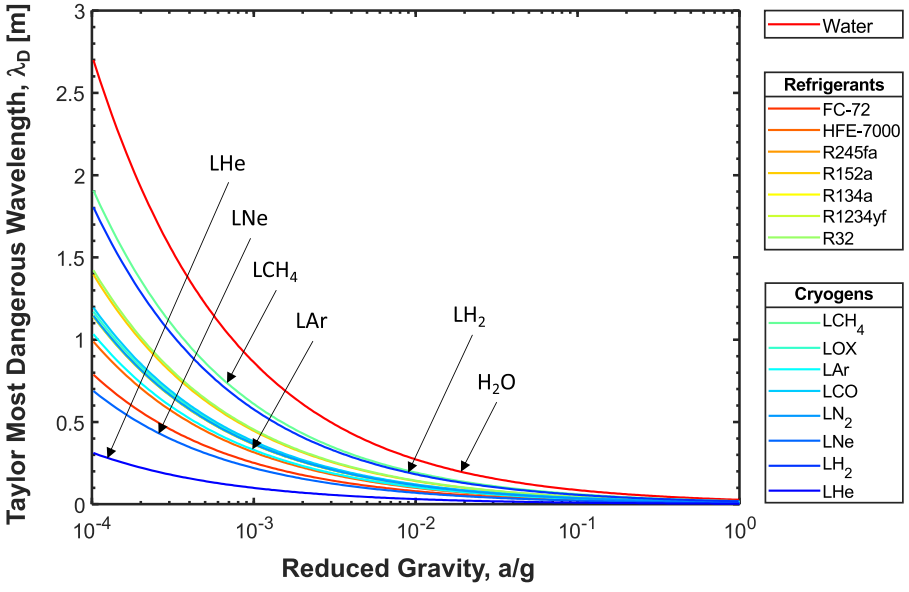

Fig. 18. Variation of Taylor Most Dangerous Wavelength with reduced gravity for different fluids at atmospheric pressure.

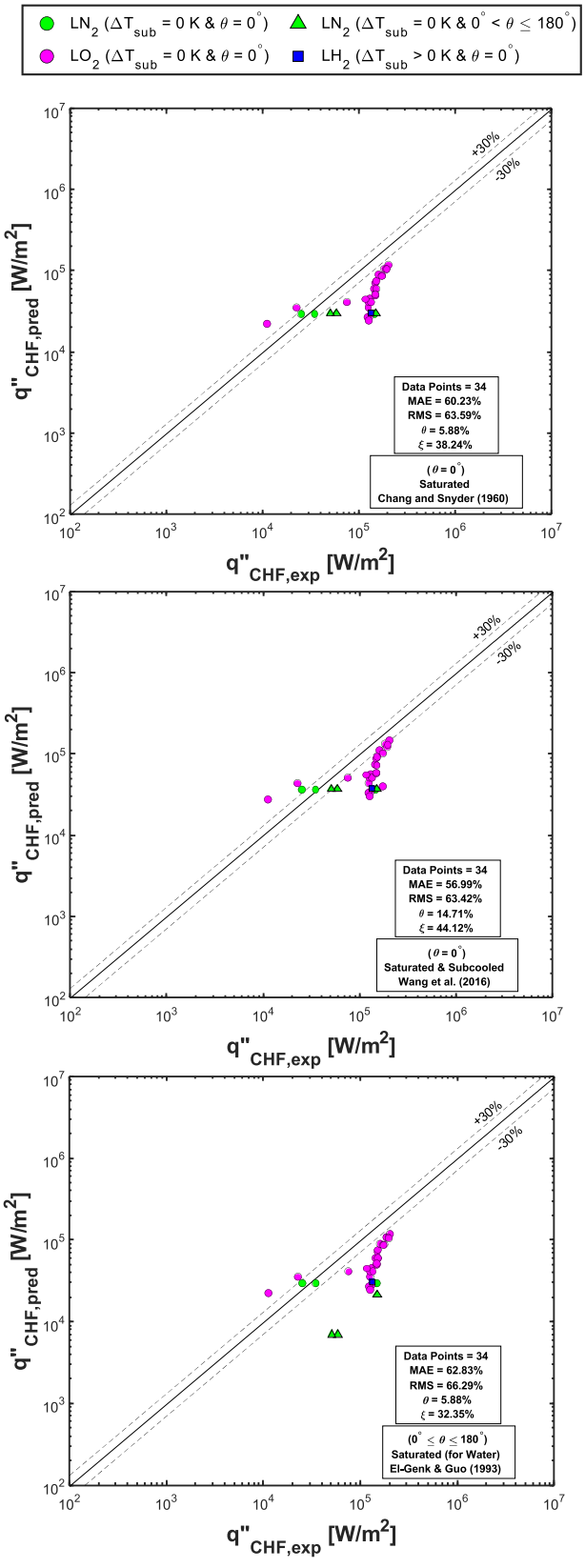

Fig. 19. Assessment of CHF correlations for saturated and subcooled pool boiling at different orientations, which also account for reduced gravity.

1. Additional data for LO_2, LAr and LCH_4.
2. Additional data spanning broad ranges of subcooling.
3. Additional data for different orientation angles, especially for LO_2, LAr, LCH_4 and LH_2.
4. Additional data for reduced pressures, especially for LAr and LCH_4.
5. Additional data for different orientation angles with subcooled conditions for all fluids.
6. Additional data for different heating surface materials, thicknesses, roughness, and aging.
7 A systematic set of experiments including contact angle information for different surface materials and surface conditions.

6.3. New universal pool boiling CHF correlations for cryogenic fluids

To achieve a new reliable CHF correlation, it crucial that a sufficiently large number of data points be available to tackle dependence on key parameters. The assessment study revealedseveral deficiencies which take the form of gaps in the database as indicated in Section 6.2. This led to avoidance of attempts to include dependence on certain parameters. More specifically,

1. Dependence on contact angle is purposely avoided in the absence of accurate contact angle information for most cryogens of interest. In fact, some of the correlations in Cases 5 and 6 required use of assumed contact angle values for certain cryogens.
2. Dependence on thickness and properties of heating wall (similar to Cases 6 and 7) is also avoided because of absence of this information for vast majority of datapoints.
3. Similarly, dependence on surface roughness (similar to Case 9) is avoided because of absence of this information for vast majority of datapoints.
4. Additionally, dependence on surface size (similar to Case 10) is avoided because of the need to incorporate modification to the correlation to address the variety of shapes and sizes, rather than employ a single universal correlation.

With this strategy, the goal is to develop a new universal correlation with proven high predictive accuracy, which could be modified in future research once major gaps in the database are filled. Without the avoided dependencies, the new correlation will reflect dependence on cryogen used, and effects of pressure, surface orientation, and subcooling, which are available for the entire final Consolidated Database.

The universal correlation is developed first for pool boiling CHF of cryogenic fluids in Earth gravity using the final Consolidated Database, which contains 1188 data points for six cryogenic fluids: LHe, LH_2, LAr, LN_2, LO_2, and LCH_4. The correlation coefficients and exponents are obtained using the algorithm-based MATLAB Optimize Live Editor Task [140]. The correlation is developed using a systematic step by step strategy starting with the case of horizontal upward-facing surface and saturated conditions. After optimizing for the baseline case, two multipliers for surface orientation effects are introduced and optimized, followed by a multiplier for subcooling effects. The final correlation,

$$q''_{CHF} = \left[0.16 - 0.104\left(\frac{P}{P_c}\right)^{10}\right] \times \left[1 - 0.004\left(\frac{P}{P_c}\right)\theta\right]\left|\cos\left(\left(\frac{88}{180}\right)\theta\right)\right|^{0.364} \times \left[1 + 0.16\left(\frac{c_{p,f}\Delta T_{sub}}{h_{fg}}\right)\right] \times \left[\rho_g h_{fg}\left(\frac{\sigma g(\rho_f - \rho_g)}{\rho_g^2}\right)^{1/4}\right]. \quad (4)$$

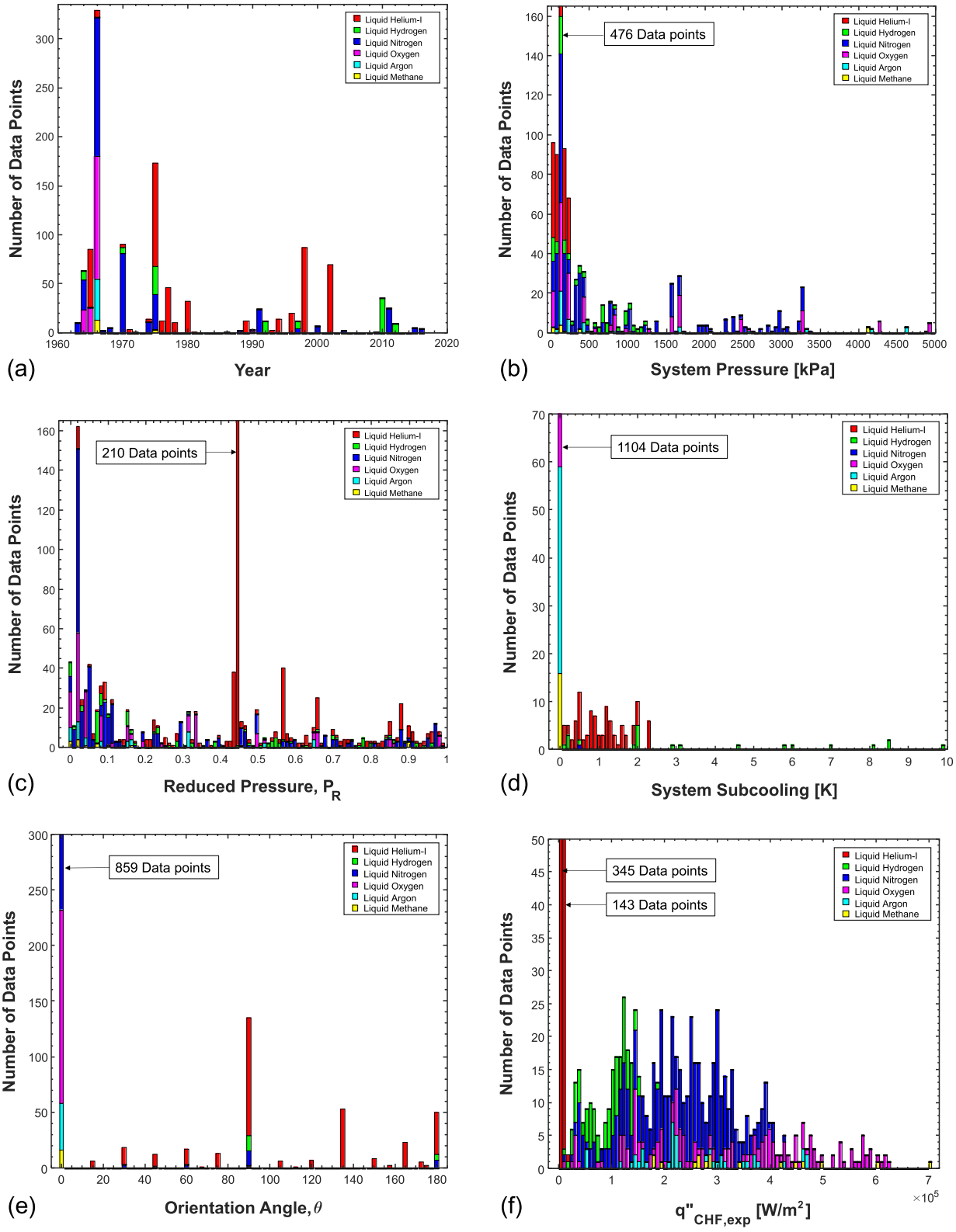

Fig. 20. Histograms of final Consolidated Database versus (a) year of study, (b) system pressure, (c) reduced pressure, (d) subcooling, (e) surface orientation, and (f) CHF magnitude.

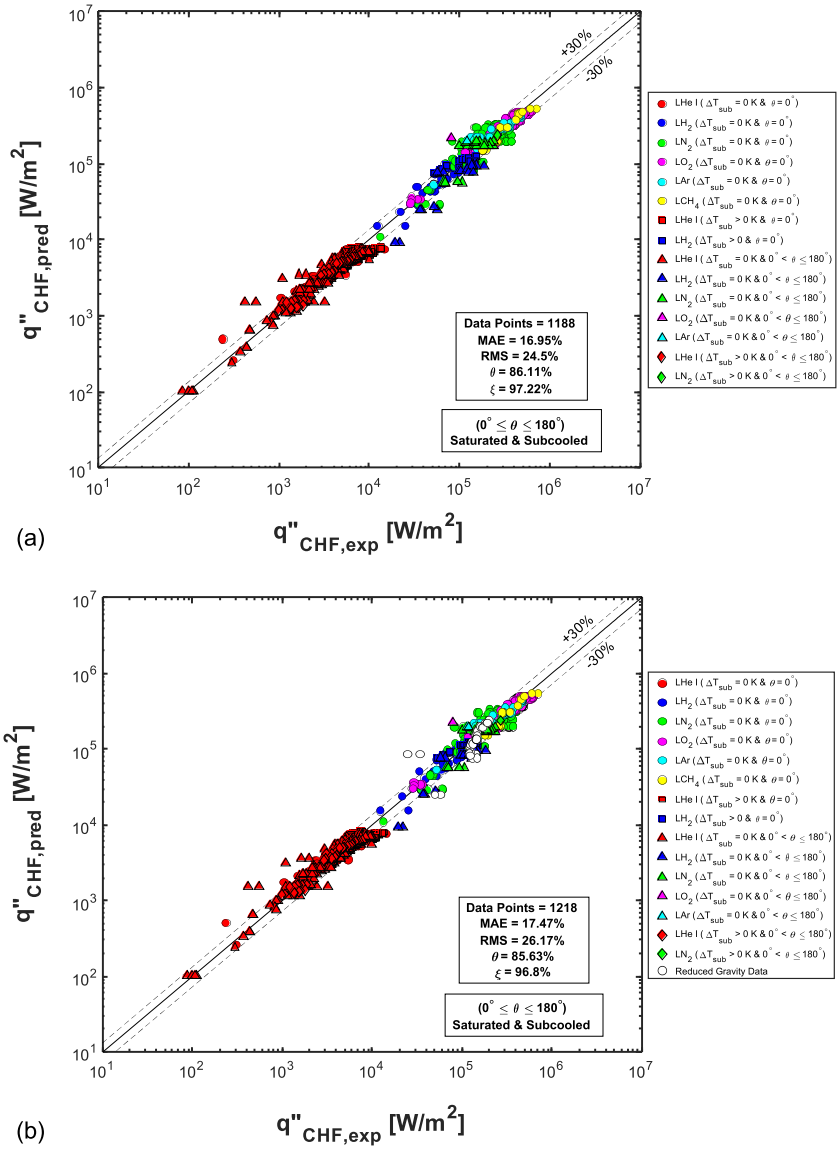

Fig. 21. Predictions of new universal pool boiling CHF correlation for cryogenic fluids for (a) Earth gravity, and (b) reduced gravity.

where θ is in degrees, has a MAE and an RMS of 16.95% and 24.5%, respectively, with 86.11% of the data predicted within 30% and 97.22% within 50%, as shown in Fig. 21(a). Notice that the correlation takes advantage of the original functional form of Kutateladze [20], which was shown earlier to provide good predictions for a majority of models and correlations. Interestingly, eliminating the data outliers in accordance with Table 8 appears to also enhance predictions of the best performing baseline Case 1 models and correlations from the initial assessment as shown in Table 9, albeit with the new correlation providing slightly better accuracy. However, as discussed later, superior accuracy of the new correlation is more strongly reflected in ability to tackle the additional impact of reduced pressure and non-horizontal surface orientations.

For the baseline case, following Wang *et al.* [29], the additional pressure term multiplier $[0.16 - 0.104(P/P_c)^{10}]$ is used to tackle high pressure effects. Next, two separate multipliers are used to account for surface orientation effects: a main cosine multiplier, $|\cos((\frac{88}{180})\theta)|^{0.364}$, capturing overall orientation trends, and a second multiplier, $[1 - 0.004(\frac{P}{P_c})\theta]$, deemed necessary to address observed data trends indicating significant influence of reduced pressure for several non-horizontal surface orientations. The latter is in addition to the pressure multiplier adopted in conjunction with the baseline case. Finally, the third multiplier, $[1 + 0.16(\frac{c_{p,f}\Delta T_{sub}}{h_{fg}})]$, is incorporated to address the subcooling effects.

After developing the universal correlation for Earth gravity, another multiplier is introduced and optimized to tackle reduced gravity effects using a small subset of 30 available data points corresponding to a reduced gravity range from 0 to 0.7466 for three cryogenic fluids: LN_2, LH_2 and LO_2.

$$q''_{CHF,reduced\ gravity} = q''_{CHF} \times \left[\frac{a}{g}\right]^{0.17} \tag{5}$$

Fig. 21(b) shows new correlation assessment results including the 30 reduced gravity datapoints. Notice that MAE with the reduced gravity parameter, 17.47%, is only slightly higher than for Earth gravity alone, 16.95%.

6.4. Comparison of new universal CHF correlation with prior CHF models and correlations

When generating the plots below for liquid helium, several important pressure and temperature limits are observed. In terms of

Table 9
Comparison of predictive accuracy of new correlation with those of best performing models and correlations from the initial assessment study for Case 1 after eliminating data outliers based on Table 8.

	MAE %	RMS %	% of points within ±30%	% of points within ±50%	Number of data points
Case 1					
Zuber and Tribus [104]	23.47	27.55	67.51	97.07	751
Lienhard and Dhir [108,109]	18.89	27.28	84.29	95.34	751
Mudawar *et al.* [18]	18.79	27.54	84.42	94.67	751
Yagov [17]	18.29	25.95	85.75	94.67	751
New CHF Correlation	***15.96***	***21.49***	***88.42***	***97.47***	***751***

Table 10
Accuracy comparison of new correlation with prior correlations at specified orientation angles.

		Mean Absolute Error (MAE) [%]												
Orientation Angle	Number of CHF data points	Chang [106]	Vishnev [116]	El-Genk and Guo (for water) [117]	El-Genk and Guo (for nitrogen) [117]	El-Genk and Guo (for helium) [117]	Arik and Bar-Cohen [119]	El-Genk and Bostanci [120]	Priarone (for FC-72) [121]	Priarone (for HFE-7100) [121]	Hata *et al.* [72]	El-Genk and Bostanci [126]	Brusstar and Merte [127,128]	New Correlation
15°	***6***	44.65	9.05	21.47	19.01	26.1	27.35	25.28	9.77	17.6	22.15	25.29	26.22	12.53
30°	***18***	41.52	15.45	23.87	21.69	27.68	26.3	28.52	14.83	21.92	23.92	28.53	24.68	18.62
45°	***12***	29.26	23.42	24.05	23.52	24.83	24.16	55.19	25.86	48.32	22.76	55.19	23.7	21.37
60°	***17***	31.41	13.19	17.82	14.27	24.88	16.55	41.56	13.83	36.53	13.36	41.59	13.63	12.66
67.5°	***1***	29.42	0.61	16.68	10.05	25.74	13.63	43.26	8.78	38.45	8.46	43.26	5.97	4.96
75°	***13***	12.16	12.38	17.28	12.15	25.52	13.81	47.39	14.07	42.44	12.01	47.43	12.27	12.16
90°	***134***	28.92	26.64	26.77	25.48	32.18	25.65	67.43	33.19	61.09	18.92	68.07	29.83	17.64
105°	***6***	12.27	18.24	12.58	15.41	21.78	14.11	75.89	29.86	65.28	12.47	75.91	25.7	15.77
112.5°	***1***	8.23	2.79	13.46	1.74	29.6	4.93	64.53	19.75	52.4	12.71	64.53	17.52	2.0
120°	***7***	23.05	27.3	16.36	25.05	21.47	22.19	99.11	42.62	81.52	14.58	99.14	42.29	23.72
135°	***53***	19.09	17.3	20.11	17.27	35.84	17.87	71.78	24.18	52.75	22.25	73.8	30.53	10.27
150°	***8***	68.78	40.45	28.32	44.57	29.96	31.41	115.46	55.75	95.94	28.64	115.49	60.09	35.25
157.5°	***2***	32.32	4.03	15.79	1.89	48.01	15.4	42.98	6.55	35.61	44.87	42.98	9.06	9.37
165°	***23***	60.92	16.83	15.85	20.7	50.35	17.13	39.15	20.27	40.82	44.15	39.16	19.57	11.07
172.5°	***5***	152.96	34.63	23.26	49.85	47.84	13.97	61.96	41.27	79.8	29.28	61.99	21.83	23.05
175°	***2***	169.9	32.99	22.62	47.67	55.7	9.89	52.41	38.41	76.15	29.8	52.41	6.16	19.41
180°	***48***	264.75	70.52	61.47	60.06	92.59	59.48	72.69	73.66	106.52	38.29	74.37	100	27.55
Avg.	***356***	***65.25***	***28.46***	***28.04***	***27.7***	***40.85***	***27.11***	***63.37***	***33.8***	***61.04***	***23.91***	***64.15***	***37.18***	***17.55***
0°	***832***	23.34	21.55	19.7	19.39	21.08	23.34	48.43	20.02	37.51	19.61	48.7	22.9	16.7

pressure, helium I has a lower pressure limit of 5.048 kPa and critical pressure of 227.46 kPa, which yield a reduced pressure range from 0.0222 to unity. In terms of temperature, helium I has λ-point temperature of 2.17 K, saturation temperature at one atmosphere of 4.2 K, critical temperature of 5.2 K, and maximum subcooling of 5.2–4.2 = 1.0 K.

Fig. 22(a) compares predictions of the new correlation for liquid helium with those of previous better performing models and correlations belonging to the baseline case. Predictions of the new correlation are very close to Kutateladze's excepting near critical pressure, but fall well within the range of other correlations Fig. 22.(b) shows predictions of the new correlation at atmospheric pressure relative to surface orientation are close to but slightly lower than those of those of Vishnev [116] Fig. 22.(c) shows CHF according to the new correlation is fairly linear with subcooling for horizontal surfaces and atmospheric pressure.

As mentioned earlier, superior performance of the new correlation is reflected in higher accuracy when tackling the additional impact of reduced pressure for non-horizontal surface orientations. A detailed comparison of predictive accuracies of the present correlation and previous better performing models and correlations that account for surface orientation is provided in Table 10. For surface orientations other than horizontal (15° to 180°), a total of 356 datapoints, the new correlation, with a MAE of 17.55% performs far better than all prior predictive tools. The same is true for horizontal surfaces ($\theta = 0$), a total of 832 datapoints, with a MAE of 16.7%.

7. Conclusions

The present study was motivated by lack of a large, reliable cryogenic pool boiling CHF database that can be used for assessment of predictive accuracy of available predictive tools - model

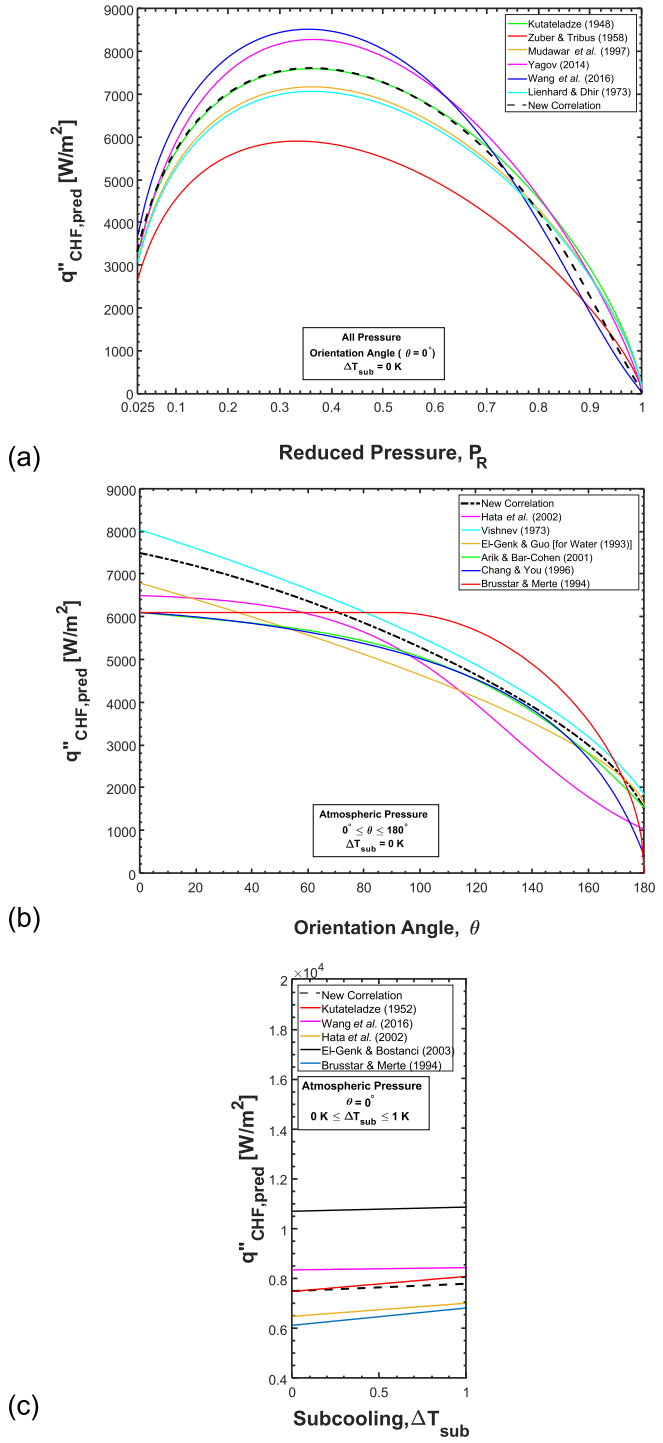

Fig. 22. Comparison of predictions of new correlation for liquid helium with previous better performing models and correlations relative to (a) pressure, (b) surface orientation, and (c) subcooling.

and correlations – or development of new tools. To do so, a new Consolidated Cryogenic Pool Boiling CHF Database for flat surfaces was compiled from world literature. Key findings from the study are as follows:

1. After initial compilation of world data, a careful assessment of individual datapoints was conducted to exclude any duplicate or questionable datapoints, resulting in an initial Consolidated Database of 1218 datapoints for six cryogenic fluids.
2. Previous models and correlations were reviewed and categorized taking into account limitations in predicting key parameters such as pressure, subcooling, and orientation of heating surface.
3. Detailed assessment of prior CHF models and correlations identified a subset that yielded fair accuracy while others produced very large deviations from the data.
4. The assessment study helped identify several data outliers, which required further exclusion of several datapoints, culminating in a final Consolidated Database consisting of 1188 datapoints, which was used to develop a new CHF correlation capable of accurately predicting CHF dependence on key parameters and cryogenic fluids of interest.
5. The new correlation shows very good predictive accuracy, with MAE and RMS of 16.95% and 24.5%, respectively, based on Earth gravity data, which comprise a large fraction of the Consolidated Database. Using a rather limited subset of 30 datapoints for three cryogens and a reduced gravity range of 0 to 0.7466, the new correlation was further modified with a reduced gravity multiplier to tackle reduced gravity conditions. The modified correlation has a MAE of 17.47%, slightly higher than for Earth gravity alone. Overall, the new correlations are proven far more accurate than all prior models and correlations.
6. CHF is strongly influenced by pressure, increasing with increasing pressure up to maximum before decreasing appreciably toward critical pressure.
7. CHF is also strongly influenced by surface orientation, and is highest for horizontal surfaces and decreases monotonically with increasing orientation angle.
8. CHF increases fairly linearly with increased subcooling for fixed pressure and surface orientation.

Declaration of Competing Interest

NONE The authors declare that they have no known competing financial interests or personal relationships that could have appeared to influence the work reported in this paper.

Acknowledgment

The authors are grateful for financial support of the National Aeronautics and Space Administration (NASA) Small Business Technology Transfer (STTR) program under a subcontract from MTS Inc. Phase I contract 80NSSC21C0266.

References

[1] V. Ganesan, R. Patel, J. Hartwig, I. Mudawar, Review of databases and correlations for saturated flow boiling heat transfer coefficient for cryogens in uniformly heated tubes, and development of new consolidated database and universal correlations, Int. J. Heat Mass Transf. 179 (2021) 121656.
[2] E.W. Lemmon, I.H. Bell, M.L. Huber, M.O. McLinden, NIST Standard Reference Database 23: Reference Fluid Thermodynamic and Transport Properties-REFPROP, Version 10.0, Standard Reference Data Program, National Institute of Standards and Technology, Gaithersburg, 2018.
[3] T.J. LaClair, I. Mudawar, Thermal transients in a capillary evaporator prior to the initiation of boiling, Int. J. Heat Mass Transfer 43 (2000) 3937–3952.
[4] G. Liang, I. Mudawar, Review of pool boiling enhancement by surface modification, Int. J. Heat Mass Transf. 128 (2019) 892–933.
[5] I. Mudawar, R.A. Houpt, Mass and momentum transport in smooth falling liquid films laminarized at relatively high Reynolds numbers, Int. J. Heat Mass Transf. 36 (1993) 3437–3448.
[6] C.O. Gersey, I. Mudawar, Effects of heater length and orientation on the trigger mechanism for near-saturated flow boiling critical heat flux—I. Photographic study and statistical characterization of the near-wall interfacial features, Int. J. Heat Mass Transf. 38 (1995) 629–641.
[7] S. Mukherjee, I. Mudawar, Pumpless loop for narrow channel and micro-channel boiling, J. Electron. Packag. 125 (2003) 431–441.
[8] S. Lee, V.S. Devahdhanush, I. Mudawar, Pressure drop characteristics of large length-to-diameter two-phase micro-channel heat sinks, Int. J. Heat Mass Transf. 115 (2017) 1258–1275.

[9] W.P. Klinzing, J.C. Rozzi, I. Mudawar, Film and transition boiling correlations for quenching of hot surfaces with water sprays, J. Heat Treat. 9 (1992) 91–103.
[10] M.E. Johns, I. Mudawar, An ultra-high power two-phase jet-impingement avionic clamshell module, J. Electron. Packag. 118 (1996) 264–270.
[11] V.S. Devahdhanush, I. Mudawar, Critical heat flux of confined round single jet and jet array impingement boiling, Int. J. Heat Mass Transf. 169 (2021) 120857.
[12] M.K. Sung, I. Mudawar, Correlation of critical heat flux in hybrid jet impingement/micro-channel cooling scheme, Int. J. Heat Mass Transf. 49 (2006) 2663–2672.
[13] W.M. Rohsenow, P. Griffith, Correlation of maximum heat transfer data for boiling of saturated liquids, Chem. Eng. Prog. Symp. Ser. 52 (1955) 47–49.
[14] N. Zuber, On the stability of boiling heat transfer, Trans. ASME 80 (1958) 711–720.
[15] Y. Haramura, Y. Katto, A new hydrodynamic model of critical heat flux, applicable widely to both pool and forced convection boiling on submerged bodies in saturated liquids, Int. J. Heat Mass Transf. 26 (1983) 389–399.
[16] T.G. Theofanous, T.N. Dinh, High heat flux boiling and burnout as microphysical phenomena: mounting evidence and opportunities, Multiph. Sci. Technol. 18 (2006) 251–276.
[17] V.V. Yagov, Is a crisis in pool boiling actually a hydrodynamic phenomenon? Int. J. Heat Mass Transf. 73 (2014) 265–273.
[18] I. Mudawar, A.H. Howard, C.O. Gersey, An analytical model for near-saturated pool boiling critical heat flux on vertical surfaces, Int. J. Heat Mass Transf. 40 (1997) 2327–2339.
[19] G. Liang, I. Mudawar, Pool boiling critical heat flux (CHF) – part 1: review of mechanisms, models, and correlations, Int. J. Heat Mass Transf. 117 (2018) 1352–1367.
[20] S.S. Kutateladze, On the transition to film boiling under natural convection, Kotloturbostroenie 3 (1948) 10–12.
[21] S.S. Kutateladze, Boiling heat transfer, Int. J. Heat Mass Transf. 4 (1961) 31–45.
[22] N. Zuber, M. Tribus, J.W. Westwater, The hydrodynamic crisis in pool boiling of saturated and subcooled liquids, in: Proceedings of the International Heat Transfer Conference, International Developments in Heat Transfer, Boulder, USA, 1961, pp. 230–236.
[23] J.E. Galloway, I. Mudawar, CHF mechanism in flow boiling from a short heated wall–I. Examination of near-wall conditions with the aid of photomicrography and high-speed video imaging, Int. J. Heat Mass Transf. 36 (1993) 2511–2526.
[24] J.E. Galloway, I. Mudawar, CHF mechanism in flow boiling from a short heated wall–II. Theoretical CHF model, Int. J. Heat Mass Transf. 36 (1993) 2527–2540.
[25] A.H. Howard, I. Mudawar, Orientation effects on pool boiling critical heat flux (CHF) and modeling of CHF for near-vertical surfaces, Int. J. Heat Mass Transf. 42 (1999) 1665–1688.
[26] V. Ganesan, R. Patel, J. Hartwig, I. Mudawar, Universal critical heat flux (CHF) correlations for cryogenic flow boiling in uniformly heated tubes, Int. J. Heat Mass Transf. 166 (2021) 120678.
[27] A. Rohatgi, WebPlotDigitizer. https://apps.automeris.io/wpd/.
[28] S. Garcia, Boiling in Liquid Hydrogen Under Gravity Compensated With a Magnetic Field, Department of Applied Physics, Chalmers University of Technology, Sweden, 2012 Masters thesis.
[29] L. Wang, Y. Li, F. Zhang, F. Xie, Y. Ma, Correlations for calculating heat transfer of hydrogen pool boiling, Int. J. Hydrog. Energy 41 (2016) 17118–17131.
[30] R.W. Graham, R.C. Hendricks, R.C. Ehlers, An experimental study of the pool heating of liquid hydrogen in the subcritical and supercritical pressure regimes over a range of accelerations, NASA Tech. Mem. TM X-52039, 1964.
[31] M. Baldwin, A. Ghavami, S.M. Ghiaasiaan, A. Majumdar, Pool boiling in liquid hydrogen, liquid methane and liquid oxygen: a review of available data and predictive tools, Cryogenics 115 (2021) 103240.
[32] C.R. Class, J.R. DeHaan, M. Piccone, R.B. Cost, Boiling heat transfer to liquid hydrogen from flat surfaces, Adv. Cryog. Eng. 5 (1960) 254–261.
[33] P. Kosky, An Experimental Study of Nucleate Boiling in Saturated Liquid Oxygen and Nitrogen Between Subatmospheric and the Critical Pressures, Department of Chemical Engineering, University of California, Berkeley, USA, 1963 MS Thesis.
[34] D.N. Lyon, P.G. Kosky, B.N. Harman, Nucleate boiling heat transfer coefficients and peak nucleate boiling fluxes for pure liquid nitrogen and oxygen on horizontal platinum surfaces from below 0.5 atmosphere to the critical pressures, Adv. Cryog. Eng. 9 (1964) 77–87.
[35] D.N. Lyon, M.C. Jones, G.L. Ritter, C.I. Chiladakis, P.G. Kosky, Peak nucleate boiling fluxes for liquid oxygen on a flat horizontal platinum surface at buoyancies corresponding to accelerations between -0.03 and 1gE, AIChE J. 11 (1965) 773–780.
[36] D.N. Lyon, Boiling heat transfer and peak nucleate boiling fluxes in saturated liquid helium between the λ and critical temperatures, Adv. Cryog. Eng. 10 (1965) 371–379.
[37] R.D. Cummings, J.L. Smith, Boiling heat transfer to liquid helium, in: Proceedings of the International Institute of Refrigeration Commission 1, Liquid Helium Technology, Boulder (U.S.A.), 1966, pp. 85–95.
[38] P.G. Kosky, Studies in Boiling Heat Transfer to Cryogenic Liquids, Department of Chemical Engineering, University of California, Berkeley, USA, 1966 PhD Dissertation.
[39] P. Kosky, D. Lyon, Pool boiling heat transfer to cryogenic liquids, AIChE J. 14 (1968) 372–387.
[40] D.N. Lyon, Pool boiling of cryogenic liquids, Adv. Cryog. Heat Transf. 64 (1968) 82–92.
[41] P.J. Marto, J.A. Moulson, M.D. Maynard, Nucleate pool boiling of nitrogen with different surface conditions, J. Heat Transf. 90 (1968) 437–444.
[42] A.P. Butler, G.B. James, B.J. Maddock, W.T. Norris, Improved pool boiling heat transfer to helium from treated surfaces and its application to superconducting magnets, Int. J. Heat Mass Transf. 13 (1970) 109–115.
[43] C. Johannes, Recent advances in heat transfer to Helium-I, in: Proceeding of the International Cryogenic Engineering Conference, Berlin, 1970, pp. 97–101.
[44] D.V. Porchey, A scanning electron microscope surface study of nucleate pool boiling heat transfer to saturated liquid nitrogen, AIChE J. 68 (1972) 162–171.
[45] D.V. Porchey, An SEM Surface Study of Nucleate Pool Boiling Heat Transfer to Saturated Liquid Nitrogen Reduced Pressures From 0.1 to 0.9, Department of Chemical Engineering, University Missouri, Rolla, USA, 1970 PhD Dissertation.
[46] H. Merte, E. Oker, J.W. Littles, Boiling heat transfer to LN2 and LH2: influence of surface orientation and reduced body forces, Prog. Refrig. Sci. Technol. (1973) 191–196.
[47] H. Merte, Incipient and Steady Boiling of Liquid Nitrogen and Liquid Hydrogen Under Reduced Gravity, Heat Transfer Laboratory, The University of Michigan, Ann Arbor, Michigan, 1970 Technical Report No. 7 (07461-51-T).
[48] M. Jergel, R. Stevenson, Contribution to the static heat transfer to boiling liquid helium, Cryogenics 14 (1974) 431–433.
[49] M. Jergel, R. Stevenson, Static heat transfer to liquid helium in open pools and narrow channels, Int. J. Heat Mass Transf. 14 (1971) 2099–2107.
[50] M. Jergel, R. Stevenson, Heat transfer to boiling helium from aluminum surfaces, Cryogenics 12 (1972) 312–313.
[51] H. Ackermann, L. Bewilogua, R. Knöner, B. Kretzschmar, I.P. Usyugin, H. Vinzelberg, Heat transfer in liquid nitrogen—methane mixtures under pressure, Cryogenics 15 (1975) 657–659.
[52] D. Warner, E.L. Park, Effect of heat transfer surface aging on heat flux in nucleate boiling liquid nitrogen, Adv. Cryog. Eng. 20 (1975) 300–303.
[53] V.A. Grigor'ev, Y.M. Pavlov, Y.V. Ametistov, A.V. Klimenko, V.V. Klimenko, Concerning the influence of thermal properties of heating surface material on heat transfer intensity of nucleate pool boiling of liquids including cryogenic ones, Cryogenics 17 (1977) 94–96.
[54] V.A. Grigor'ev, Y.M. Pavlov, Y.V. Ametistov, V.I. Antipov, Heat transfer in boiling helium to superconducting elements in power-generating equipment, future energy production systems, Heat Mass Transf. Process. 1 (1976) 261–268.
[55] H. Kobayashi, K. Yasukochi, K. Tokuyama, Heat transfer to liquid helium in a narrow channel below 4.2 K, in: Proceedings of the International Cryogenic Engineering Conference, Grenoble, 1976, pp. 307–309.
[56] H. Ogata, W. Nakayama, Heat transfer to subcritical and supercritical helium in centrifugal acceleration fields 1. Free convection regime and boiling regime, Cryogenics 17 (1977) 461–470.
[57] H. Ogata, W. Nakayama, Heat transfer to boiling helium from machined and chemically treated copper surfaces, Adv. Cryog. Eng. 27 (1981) 309–317.
[58] Y.A. Kirichenko, K.V. Rusanov, E.G. Tyurina, Investigation of burnouts for boiling nitrogen with free motion in vertical plane-parallel channels, Therm. Eng. 31 (1984) 140–142.
[59] Z. Chen, S.W. Van Sciver, Channel heat transfer in He I - steady state orientation dependence, Adv. Cryog. Eng. 31 (1986) 431–438.
[60] B. Jager, G. Bon Mardion, G. Claudet, M. Desmaris, Heat transfer in He I for industrially manufactured aluminum plate heat exchangers, Cryogenics 26 (1986) 222–225.
[61] C. Beduz, R.G. Scurlock, A.J. Sousa, Angular dependence of boiling heat transfer mechanisms in liquid nitrogen, Adv. Cryog. Eng. 33 (1988) 363–370.
[62] G.R. Chandratilleke, S. Nishio, H. Ohkubo, Pool boiling heat transfer to saturated liquid helium from coated surface, Cryogenics 29 (1989) 588–592.
[63] S.P. Ashworth, C. Beduz, J. Mayne, A. Pasek, R.G. Scurlock, Evaluation of a novel enhanced boiling surface in cryogenic liquids, Adv. Cryog. Eng. 35 (1990) 429–435.
[64] H. Ogata, H. Mori, Steady state heat transfer in transition boiling of helium on copper surfaces, Cryogenics 33 (1993) 640–642.
[65] A. Iwamoto, T. Mito, K. Takahata, N. Yanagi, J. Yamamoto, Heat transfer of a large copper plate to liquid helium application to large scale superconductors, Cryogenics 34 (1994) 321–324.
[66] R.G. Scurlock, Enhanced boiling heat transfer surfaces, Cryogenics 35 (1995) 233–237.
[67] V. Drach, J. Fricke, Transient heat transfer from smooth surfaces into liquid nitrogen, Cryogenics 36 (1996) 263–269.
[68] Y. Huang, S.W. Van Sciver, Heat transfer from aluminum surfaces to pool boiling He I, Adv. Cryog. Eng. 41 (1996) 211–216.
[69] A. Iwamoto, T. Mito, K. Takahata, N. Yanagi, J. Yamamoto, Heat transfer from an oxidized large copper surface to liquid helium: dependence on surface orientation and treatment, Adv. Cryog. Eng. 41 (1996) 217–224.
[70] D.N.T. Nguyen, R.H. Chen, L.C. Chow, C. Gu, Effects of heater orientation and confinement on liquid nitrogen pool boiling, J. Thermophys. Heat Transf. 14 (2000) 109–111.
[71] H. Tatsumoto, K. Hata, K. Hama, Y. Shirai, M. Shiotsu, Critical heat fluxes on a flat plate attached to one end of a rectangular duct containing pressurized He II, Adv. Cryog. Eng. 45 (2000) 1073–1080.
[72] K. Hata, H. Nakagawa, H. Tatsumoto, Y. Shirai, M. Shiotsu, Critical heat flux on a flat plate in a pool of subcooled liquid helium, Proc. Am. Inst. Phys. 613 (2002) 1460–1467.
[73] K. Ohira, H. Furumoto, Nucleate pool boiling heat transfer to slush hydrogen, in: Proceedings of the International Cryogenic Engineering/International Cryogenic Materials Conference, 1997, pp. 601–604.

[74] M.I. Delov, K.V. Kutsenko, A.A. Lavrukhin, Effect of orientation of the heat-release surface on heat transfer to liquid nitrogen, Bull. Lebedev Phys. Inst. 41 (2014) 196–199.
[75] B.V. Balakin, M.I. Delov, K.V. Kutsenko, A.A. Lavrukhin, O.V. Zhdaneev, Heat transfer from Ni-W tapes in liquid nitrogen at different orientations in the field of gravity, Cryogenics 65 (2015) 5–9.
[76] E.A. Ibrahim, R.W. Boom, G.E. McIntosh, Heat transfer to subcooled liquid helium, Adv. Cryog. Eng. 23 (1978) 333–339.
[77] S.M. Kozlov, S.V. Nozdrin, Heat transfer and boundaries of its regimes during hydrogen boiling at different metallic surfaces, Cryogenics 32 (1992) 245–248.
[78] Y. Shirai, H. Tatsumoto, M. Shiotsu, K. Hata, H. Kobayashi, Y. Naruo, Y. Inatani, Boiling heat transfer from a horizontal flat plate in a pool of liquid hydrogen, Cryogenics 50 (2010) 410–416.
[79] Y. Shirai, H. Tatsumoto, K. Hata, M. Shiotsu, H. Kobayashi, Y. Naruo, Y. Inatani, Preliminary study on heat transfer characteristics of liquid hydrogen for coolant of HTC superconductors, Proc. Am. Inst. Phys. 1218 (2010) 337–344.
[80] L. Bewilogua, R. Knöner, H. Vinzelberg, Heat transfer in cryogenic liquids under pressure, Cryogenics 15 (1975) 121–125.
[81] I.P. Vishnev, I.A. Filatov, Ya.G. Vinokur, v.V. Gorokhov, G.G. Svalov, Study of heat transfer in boiling of helium on surfaces with various orientations, Heat Transf. Sov. Res. 8 (1976) 104–108.
[82] V.I. Deev, V.E. Keilin, I.A. Kovalev, A.K. Kondratenko, V.I. Petrovichev, Nucleate and film pool boiling heat transfer to saturated liquid helium, Cryogenics 17 (1977) 557–562.
[83] B.I. Verkin, Yu.A. Kirichenko, S.M. Kozlov, K.V. Rusanov, Heat transfer during pool boiling of subcooled helium, in: Proceedings of the International Cryogenic Engineering Conference, Genova , Italy, 1980, pp. 256–260.
[84] S. Nishio, G.R. Chandratilleke, Steady-state pool boiling heat transfer to saturated liquid helium at atmospheric pressure, JSME Int. J. Ser. 2 32 (1989) 639–645 Fluids Eng., Heat Transfer, Power, Combustion, Thermophys Properties..
[85] A. Iwamoto, R. Maekawa, T. Mito, J. Yamamoto, Steady state heat transfer characteristics in He I with different surface area, Adv. Cryog. Eng. 43 (1998) 1481–1487.
[86] V.A. Grigor'ev, Y.M. Pavlov, Y.V. Ametistov, An investigation of nucleate boiling heat transfer of helium, in: Proceedings of the International. Heat Transfer Conference 5, Tokyo, 1974, pp. 45–49. B2.3.
[87] A. Iwamoto, R. Maekawa, T. Mito, S. Satoh, Heat transfer characteristics of liquid helium with different surface width and length, in: Proceedings of the International. Cryogenic Engineering, Bomemouth , England, 1998, pp. 801–804.
[88] E.W. Lewis, J.A. Clark, H. Merte, Boiling of Liquid Nitrogen in Reduced Gravity Fields With Subcooling, Department of Mechanical Engineering, Heat Transfer Laboratory, The University of Michigan, Ann Arbor, 1967 Technical Report No. 2, Report 07461-20-T.
[89] F.D. Akhmedov, V.A. Grigor'ev, A.S. Dudkevich, The boiling of nitrogen at pressures from atmospheric to critical, Therm. Eng. 21 (1974) 120–121.
[90] J.L. Swanson, H.F. Bowman, Transient surface temperature behavior in nucleate pool-boiling nitrogen, Heat Transf. 4 (1974) 60–64.
[91] S. Ishigai, M. Kaji, T. Watanabe, A. Yamaji, Pool boiling heat transfer from horizontal plates to liquid nitrogen under atmospheric pressure, Technol. Rep. Osaka Univ. 27 (1977) 485–496.
[92] S. Nishio, Study on the minimum heat flux point for boiling heat transfer on a horizontal flat plate (effects of transients and thermal conductance of surface), Heat Transf. Jpn. Res. 15 (1986) 15–33.
[93] Y.A. Kirichenko, S.M. Kozlov, K.V. Rusanov, E.G. Tyurina, Heat transfer crisis during liquid nitrogen cooling of high temperature superconductor, Cryogenics 31 (1991) 979–984.
[94] M.C. Duluc, B. Stutz, M. Lallemand, Transient nucleate boiling under stepwise heat generation for highly wetting fluids, Int. J. Heat Mass Transf. 47 (2004) 5541–5553.
[95] T. Jin, J.P. Hong, H. Zheng, K. Tang, Z.H. Gan, Measurement of boiling heat transfer coefficient in liquid nitrogen bath by inverse heat conduction method, J. Zhejiang Univ. Sci. A 10 (2009) 691–696.
[96] P. Wang, P.L. Lewin, D.J. Swaffield, G. Chen, Electric field effects on boiling heat transfer of liquid nitrogen, Cryogenics 49 (2009) 379–389.
[97] T. Jin, S.Y. Zhang, K. Tang, Y.Z. Huang, Observation and analysis of the detachment frequency of coalesced bubbles in pool boiling liquid nitrogen, Cryogenics 51 (2011) 516–520.
[98] C. Bombardieri, C. Manfletti, Influence of wall material on nucleate pool boiling of liquid nitrogen, Int. J. Heat Mass Transf. 94 (2016) 1–8.
[99] A. Zoubir, R. Agounoun, I. Kadiri, K. Sbai, M. Rahmoune, Experimental study of the intensification of heat transfer by pool boiling LN2: application to cooling of a brass ribbon in horizontal position, Front. Heat Mass Transf. 7 (2016) 1–6.
[100] M. Shiotsu, K. Hata, A. Sakurai, C. Suzawa, S. Isojima, K. Sato, Transient heat transfer from a silver sheathed high-Tc superconducting tape in liquid nitrogen, in: Proceedings of the 16th International Cryogenic Engineering Conference/International Cryogenic Materials Conference, Kitakyushu, Japan, 1997, pp. 617–620.
[101] L. Wang, K. Zhu, F. Xie, Y. Ma, Y. Li, Prediction of pool boiling heat transfer for hydrogen in microgravity, Int. J. Heat Mass Transf. 94 (2016) 465–473.
[102] B.N. Harman, M.S. Thesis, University of California, Berkeley, USA, 1960.
[103] V.M. Borishanskii, An equation generalizing experimental data on the cessation of bubble boiling in a large volume of liquid, Soviet physics - technical physics, Am. Inst. Phys. 1 (1956) 438–442.
[104] N. Zuber, M. Tribus, Further remarks on the stability of boiling heat transfer, Report No. 58-5, United States, 1958.
[105] Y.P. Chang, N.W. Snyder, Heat transfer in saturated boiling, Chem. Eng. Prog. Symp. Ser. 56 (1960) 25–38.
[106] Y.P. Chang, An Analysis of the Critical Conditions and Burnout in Boiling heat Transfer, University of Notre Dame, Notre Dame, 1961 Report no. TID-14004.
[107] R. Moissis, P.J. Berenson, On the hydrodynamic transitions in nucleate boiling, J. Heat Transf. 85 (1963) 221–226.
[108] J.H. Lienhard, V.K. Dhir, Extended Hydrodynamic Theory of the Peak and Minimum Pool Boiling Heat Fluxes, NASA report CR-2270, NASA, 1973.
[109] J.H. Lienhard, V.K. Dhir, Hydrodynamic prediction of peak pool-boiling heat fluxes from finite bodies, J. Heat Transf. 95 (1973) 152–158.
[110] R.I. Soziev, M.A. Khrizolitova, Calculating critical heat flux density with pool boiling, Therm. Eng. 36 (1989) 400–401.
[111] H. Sakashita, A. Ono, Boiling behaviors and critical heat flux on a horizontal plate in saturated pool boiling of water at high pressures, Int. J. Heat Mass Transf. 52 (2009) 744–750.
[112] A.K. Rajvanshi, J.S. Saini, R. Prakash, Investigation of macrolayer thickness in nucleate pool boiling at high heat flux, Int. J. Heat Mass Transf. 35 (1992) 343–350.
[113] T. Kumada, H. Sakashita, Pool boiling heat transfer-II. Thickness of liquid macrolayer formed beneath vapor masses, Int. J. Heat Mass Transf. 38 (1995) 979–987.
[114] W. Bailey, E. Young, C. Beduz, Y. Yang, Pool boiling study on candidature of pentane, methanol and water for near room temperature cooling, in: Proceedings of the Thermal and Thermomechanical Phenomena in Electronic Systems, IEEE, San Diego, USA, 2006, pp. 599–603.
[115] C.K. Guan, J.F. Klausner, R. Mei, A new mechanistic model for pool boiling CHF on horizontal surfaces, Int. J. Heat Mass Transf. 54 (2011) 3960–3969.
[116] I.P. Vishnev, Effect of orienting the hot surface with respect to the gravitational field on the critical nucleate boiling of a liquid, J. Eng. Phys. 24 (1973) 43–48.
[117] M.S. El-Genk, Z. Guo, Transient boiling from inclined and downward-facing surfaces in a saturated pool, Int. J. Refrig. 16 (1993) 414–422.
[118] J.Y. Chang, S.M. You, Heater orientation effects on pool boiling of micro–porous-enhanced surfaces in saturated FC-72, J. Heat Transf. 118 (1996) 937–943.
[119] M. Arik, A. Bar-Cohen, Ebullient cooling of integrated circuits by Novec fluids, in: Proceedings of the Pacific Rim/ASME International Intersociety Electronic Packaging Confernce, Hawaii, USA, 2001.
[120] M.S. El-Genk, H. Bostanci, Saturation boiling of HFE-7100 from a copper surface, simulating a microelectronic chip, Int. J. Heat Mass Transf. 46 (2003) 1841–1854.
[121] A. Priarone, Effect of surface orientation on nucleate boiling and critical heat flux of dielectric fluids, Int. J. Therm. Sci. 44 (2005) 822–831.
[122] S.S. Kutateladze, Heat Transfer in Condensation and Boiling, U.S. Atomic Energy Commission, 1952 Moscow, english translationAEC-tr-3770.
[123] C.F. Bonilla, Heat removal, in: Nuclear Engineering, McGraw-Hill, New York, 1957, pp. 399–431.
[124] H.J. Ivey, D.J. Morris, On the Relevance of the Vapor-Liquid Exchange Mechanism for Sub-Cooled Boiling Heat Transfer at High Pressure, AEEW, 1962 UK ReportR-137, Winfrith.
[125] E.G. Brentari, Boiling Heat Transfer for Oxygen, Nitrogen, Hydrogen, and Helium, National Bureau of Standards report NBS-317, Gaithersburg, MD, 1965.
[126] M.S. El-Genk, H. Bostanci, Combined effects of subcooling and surface orientation on pool boiling of HFE-7100 from a simulated electronic chip, Exp. Heat Transf. 16 (2003) 281–301.
[127] M.J. Brusstar, H. Merte, Effects of buoyancy on the critical heat flux in forced convection, J. Thermophys. Heat Transf. 8 (1994) 322–328.
[128] M.J. Brusstar, H. Merte, Effects of heater surface orientation on the critical heat flux-II. A model for pool and forced convection subcooled boiling, Int. J. Heat Mass Transf. 40 (1997) 4021–4030.
[129] Y.A. Kirichenko, P.S. Chernyakov, Determination of the first critical thermal flux on flat heaters, J. Eng. Phys. Thermophys. 20 (1971) 699–703.
[130] S.J. Kim, I.C. Bang, J. Buongiorno, L.W. Hu, Surface wettability change during pool boiling of nanofluids and its effect on critical heat flux, Int. J. Heat Mass Transf. 50 (2007) 4105–4116.
[131] S.G. Kandlikar, A theoretical model to predict pool boiling CHF incorporating effects of contact angle and orientation, J. Heat Transf. 123 (2001) 1071–1079.
[132] L. Liao, R. Bao, Z. Liu, Compositive effects of orientation and contact angle on critical heat flux in pool boiling of water, Heat Mass Transf. 44 (2008) 1447–1453.
[133] I. Golobič, A.E. Bergles, Effects of heater-side factors on the saturated pool boiling critical heat flux, Exp. Therm. Fluid Sci. 15 (1997) 43–51.
[134] A.A. Watwe, A. Bar-Cohen, Modeling of conduction effects on pool boiling critical heat flux of dielectric liquids, in: Proceedings of the 32nd National Heat Transfer Conference, Baltimore, USA, 1997.
[135] J.M. Ramilison, P. Sadasivan, J.H. Lienhard, Surface factors influencing burnout on flat heaters, J. Heat Transf. 114 (1992) 287–290.
[136] J. Kim, S. Jun, R. Laksnarain, S.M. You, Effect of surface roughness on pool boiling heat transfer at a heated surface having moderate wettability, Int. J. Heat Mass Transf. 101 (2016) 992–1002.
[137] P.J. Brennan, E.A. Skrabek, Design and Development of a Prototype Static Cryogenic Heat Transfer System, NASA, 1971 NASA report CR-121939.

[138] K. Bellur, V. Konduru, M. Kulshreshtha, D. Tyrewala, E. Medici, J.S. Allen, C.K. Choi, D.S. Hussey, D.C. Jacobson, J.B. Leão, J. McQuillen, J. Hermanson, A. Tamilarasan, Contact angle measurement of liquid hydrogen (LH2) in stainless steel and aluminum cells, J. Heat Transf. 138 (2016), doi:10.1115/1.4032232.

[139] V. Konduru, K. Bellur, E.F. Médici, J.S. Allen, C.K. Choi, D.S. Hussey, D. Jacobson, J.B. Leão, J. McQuillen, J.C. Hermanson, Examining liquid hydrogen wettability using neutron imaging, J. Heat Transf. 138 (2016), doi:10.1115/1.4033822.

[140] MATLAB Optimize Live Editor Task, R2021a, Version 9.10.0.1602886, The MathWorks, Inc., Natick, MA, 2021.